Electronic Supplementary Material (ESI) for Catalysis Science & Technology.

Supplementary Information

Catalytic Hydrogenation of CO_2 to Methanol in a Lewis Pair Functionalized MOF

Jingyun Ye[a], J. Karl Johnson[a,b]*

[a]Department of Chemical & Petroleum Engineering, University of Pittsburgh, Pittsburgh, Pennsylvania 15261, United States
[b]Pittsburgh Quantum Institute, Pittsburgh, Pennsylvania 15261, United States

*E-mail: karlj@pitt.edu

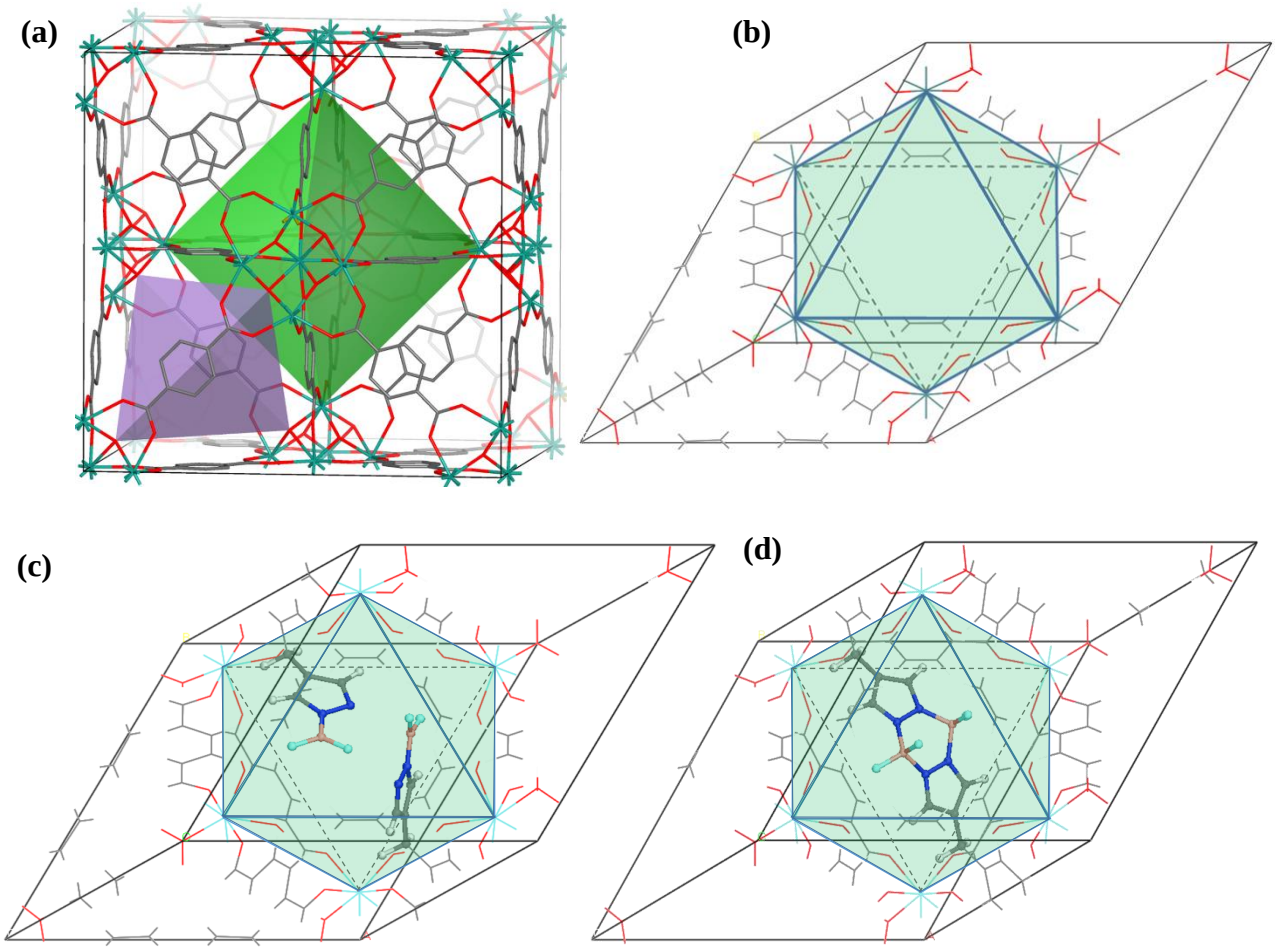

Fig. S1 Lewis pair functionalized UiO-66. (a) Octahedral cage (green) and tetrahedral cage (purple) of the unit cell of UiO-66. (b) Primitive cell of UiO-66 with the octahedral cage highlighted. Two Lewis pair functional groups in a single UiO-66 primitive cell with the groups (c) unquenched and (d) quenched. The energy of the quenched configuration is 1.74 eV lower than the unquenched configuration. The UiO-66 framework atoms are represented by lines, and the Lewis pair functional moieties are represented by balls and sticks. Atom colors: gray for C, red for O, blue for N, pink for B, dark green for Zr, light blue for F. Hydrogen atoms belonging to the framework are not shown for clarity.

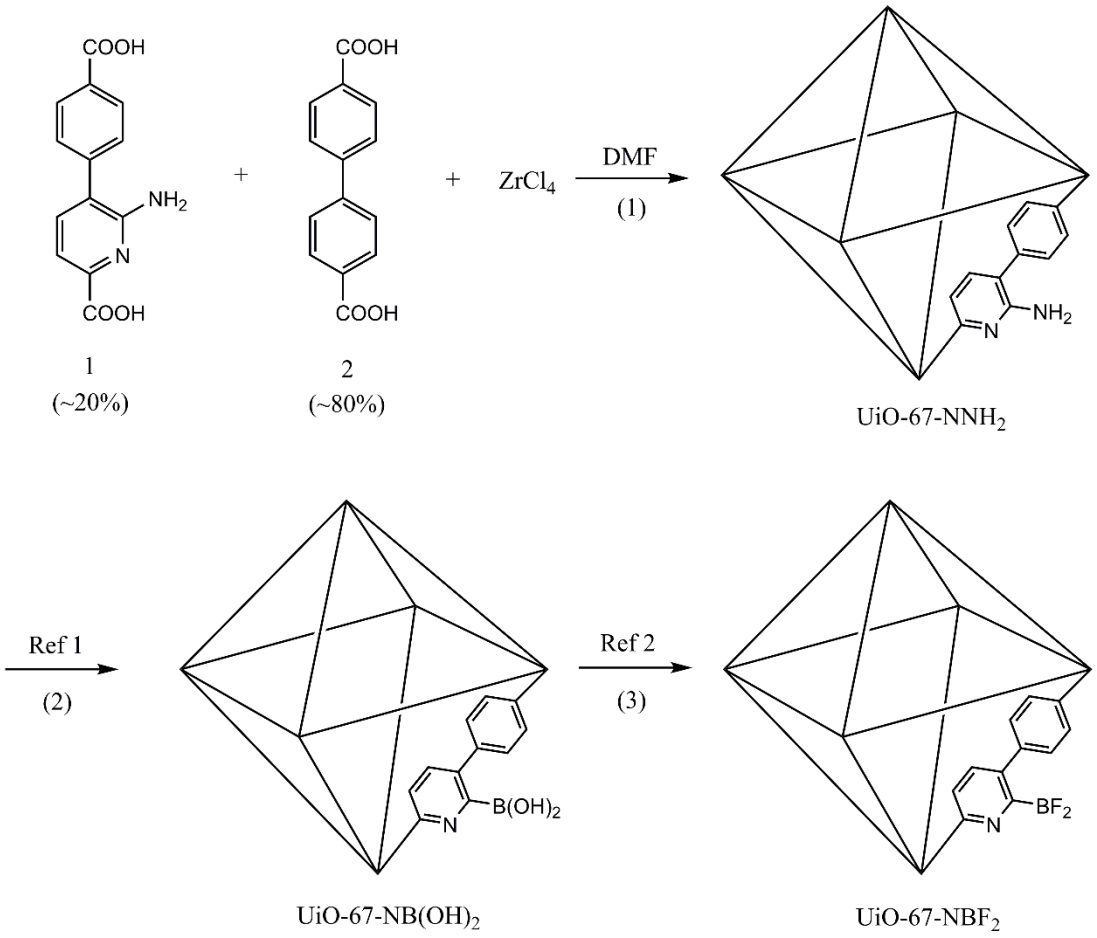

Scheme S1. Proposed synthesis route for UiO-67-NBF_2.[1-2]

We here sketch out a potential pathway for synthesis of UiO-67-NBF_2 as shown in Scheme S1. NH_2 functionalized PBDC (PBDC: 1,4-benzenedicarboxylate) [3-8] and N doped PBDC [9-12] are well known linkers can be synthesized for MOF. The linker shown in Scheme S1, 2-amino-3-(4-carboxyphenyl)pyridine-6-carboxylic acid, **1** may be obtained by modification of dcppy with N.[13]

(1) Synthesis of UiO-67-N-NF_2 is achievable based on the postsynthetic modification (PSM) method for synthesis of UiO-67-dcppy (dcppy: 2-phenylpyridine-5,4 0-dicarboxylic acid).[14] Here, we can combine PBDC and **1** to get a statistical mixture of linker and finally UiO-67-N-NH_2 obtained should be partially functionalized by N-NH_2.
(2) The NH_2 group may be replaced with a $B(OH)_2$ functional group using chemistry described by Zhao et al. in Ref 1 for producing arylbornic acids from arylamines.
(3) The $B(OH)_2$ group can be modified to BF_2 through Method A described by Ishihara et al. in Ref 2 to obtain the target product UiO-67-NBF_2.

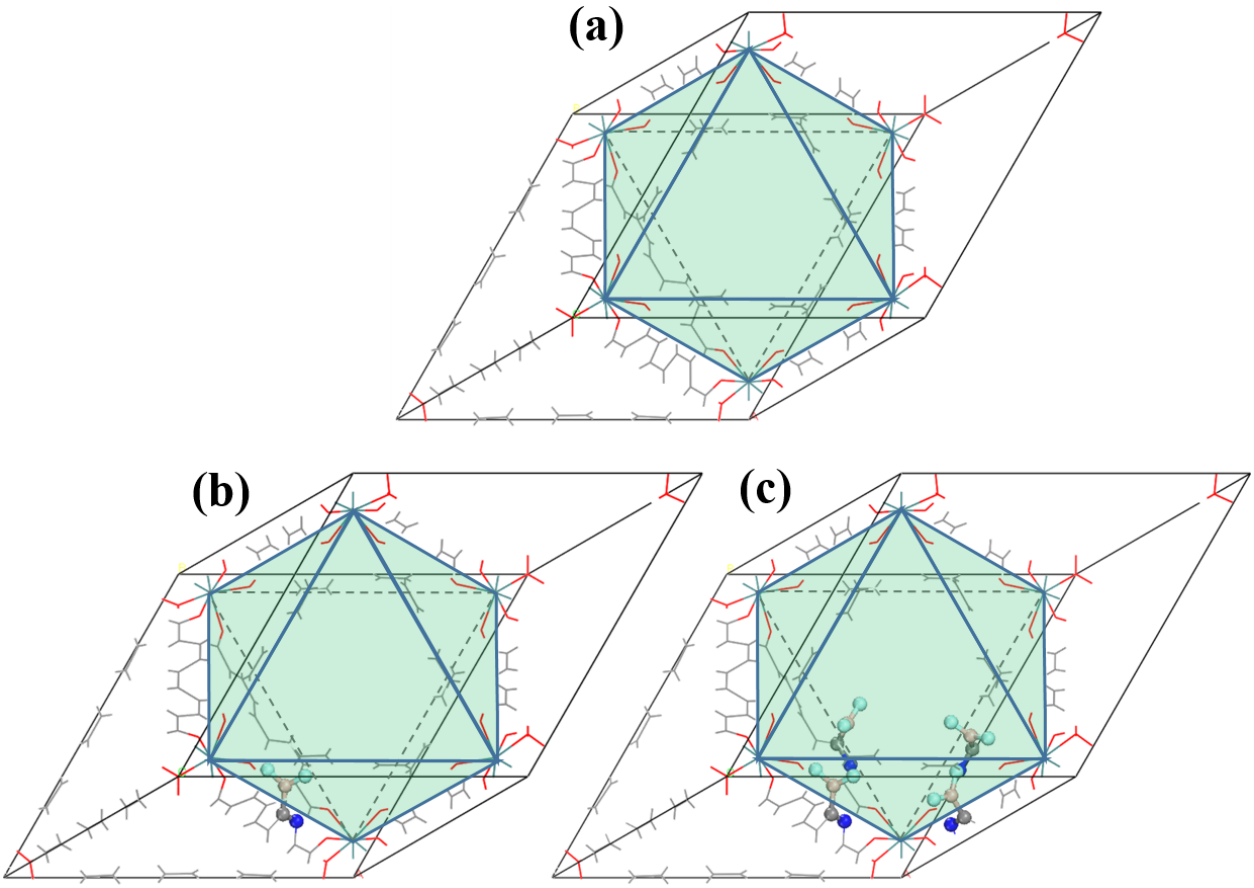

Fig. S2 Primitive cell of (a) UiO-67, (b) UiO-67-NBF_2 and (c) UiO-67-$(NBF_2)_4$ with the octahedral cage highlighted

Table S1. Summary of pore volumes and porosities for UiO-67, UiO-67-NBF_2 and UiO-67-$(NBF_2)_4$ calculated by PLATON[15].

Material	Pore volume (Å^3)	Porosity (%)
UiO-67	3360.7	68.2(67.7[16])
UiO-67-NBF_2	3340.2	67.8
UiO-67-$(NBF_2)_4$	3269.1	66.3

The pore volume of UiO-67 simulated is 3360.7 Å^3/primitive cell (0.955 cm^3/g), which is close to the experimental results 0.85 cm^3/g [17] and simulated results 1.05 cm^3/g [18].

Table S2. The adsorption energies of CO_2 and H_2 in UiO-67-X, with X= NBF_2, NBH_2, $NBCl_2$, $NB(CH_3)_2$, $NB(Ph)_2$.

E_{ads}	H_2	CO_2
UiO-67-NBF_2	-0.50	-0.20
UiO-67-NBH_2	-1.35	-0.80
UiO-67-$NBCl_2$	-0.99	-0.26
UiO-67-$NB(CH_3)_2$	-0.45	-0.18
UiO-67-$NB(Ph)_2$	-0.21	0.14

Note: Ph = phenyl group

Table S3. The structural details of CO_2 and H_2 adsorbed in UiO-67-X. (bond length: d/angstrom, angle: ∠/degree)

	CO_2					**H_2**		
	$d_{(C-O_a)}$	$d_{(C-O_b)}$	$\angle_{(O_a-C-O_b)}$	$d_{(O_a-B)}$	$d_{(C-N_2)}$	$d_{(H_a-H_b)}$	$d_{(H_a-B)}$	$d_{(H_b-N_2)}$
Free H_2						0.732		
Free CO_2	1.176	1.176	180.0					
UiO-67-NBF_2	1.289	1.193	130.8	1.530	1.646	2.041	1.232	1.031
UiO-67-NBH_2	1.293	1.198	129.1	1.582	1.604	2.121	1.220	1.027
UiO-67-$NBCl_2$	1.302	1.193	129.3	1.509	1.603	2.080	1.211	1.029
UiO-67-$NB(CH_3)_2$	1.285	1.194	129.8	1.554	1.613	2.019	1.233	1.029
UiO-67-$NB(Ph)_2$	1.288	1.194	131.4	1.549	1.648	2.055	1.231	1.032

Table S4. The structural details of CO_2 and H_2 adsorbed in UiO-67-X. (bond length: d/angstrom, angle: ∠/degree)

				CO_2			**H_2**		
	$d_{(C-N)}$	$d_{(C-B)}$	$\angle_{(N-C-B)}$	$d_{(C-N)}$	$d_{(C-B)}$	$\angle_{(N-C-B)}$	$d_{(C-N)}$	$d_{(C-B)}$	$\angle_{(N-C-B)}$
UiO-67-NBF_2	1.351	1.576	112.8	1.358	1.628	110.0	1.351	1.659	112.4
UiO-67-NBH_2	1.377	1.597	120.6	1.367	1.582	110.2	1.367	1.589	114.9
UiO-67-$NBCl_2$	1.353	1.572	112.0	1.365	1.619	108.7	1.360	1.627	111.5
UiO-67-$NB(CH_3)_2$	1.357	1.583	112.4	1.370	1.610	110.0	1.369	1.623	112.4
UiO-67-$NB(Ph)_2$	1.352	1.570	114.3	1.360	1.623	110.4	1.356	1.656	111.7

Table S5. The DDEC charges of Lewis acid (B) and base (N) sites of functional group in UiO-67-NBF_2 and adsorbed CO_2 or H_2. The atom labels are defined in Fig. 2.

	Lewis acid	Lewis base	CO_2			H_2	
	B	N	C	O_a	O_b	H_a	H_b
UiO-67-NBF_2	+0.78	-0.23					
w/CO_2	+0.72	-0.03	+0.63	-0.41	-0.40		
w/H_2	+0.45	-0.12				-0.24	+0.29

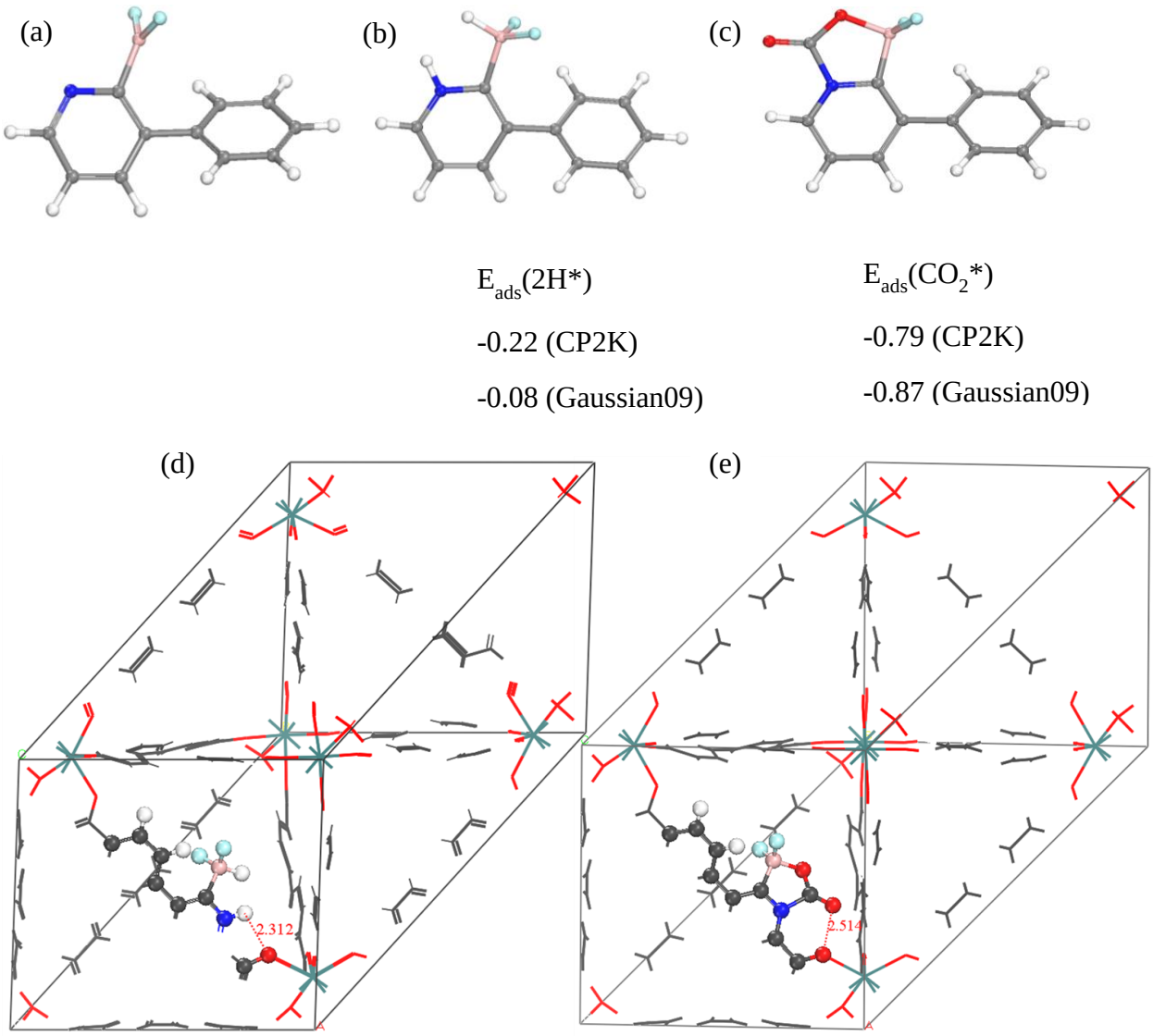

Fig. S3 The optimized cluster model of the NBF_2 functionalized BPDC ligand with carboxylate groups in BPDC ligand replaced by H atoms (a) and the NBF_2 functionalized ligand cluster with adsorbed H_2 (b) and CO_2 (c). The adsorption energies of H_2 and CO_2 calculated by CP2K and Gaussian 09.[19] The theoretical level for CP2K calcuations is described in the main text and for Gaussian calcuation we used the M062X functional with the 6-311++G(d,p) basis sets. The optimized primitive cell structure of UiO-67-NBF_2 with adsorbed H_2 and CO_2 are shown in (d) and (e), respectively, for comparison. Note the steric hinderance in (e) caused by the close approach of the two oxygen atoms, only 2.514 Å apart. In contrast, the H-O distance in (d) is appropriate for hydrogen bonding.

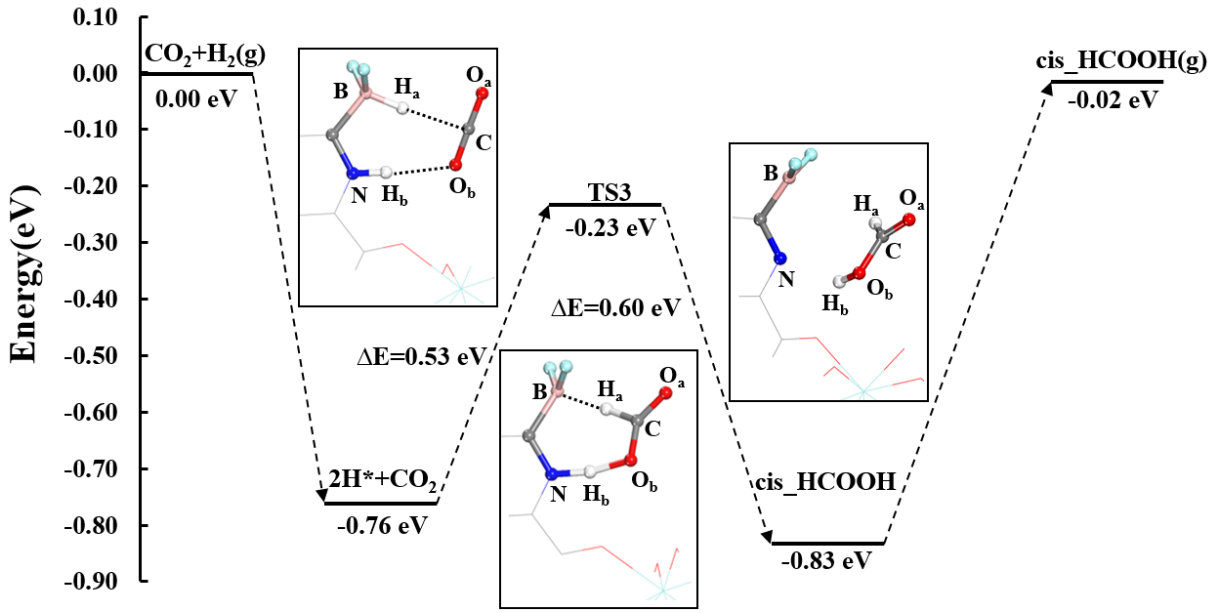

Fig. S4 Potential energy profile for CO_2 hydrogenation to produce cis-HCOOH in UiO-67-NBF_2. Structural details of 2H*+CO_2: d_{C-O_a}=1.176 Å, d_{C-O_b}=1.180 Å, $\angle O_a-C-O_b$=178.29°, $d_{O_b-H_b}$ =2.573 Å, d_{C-H_a}=2.804 Å, d_{H_b-N}=1.031 Å, d_{H_a-B}=1.233 Å; TS3: d_{C-O_a}=1.213 Å, d_{C-O_b}=1.266 Å, $\angle O_a-C-O_b$=135.96, $d_{O_b-H_b}$=1.292 Å, d_{C-H_a}=1.250 Å, d_{H_b-N}=1.242 Å, d_{H_a-B}=1.577 Å; HCOOH: d_{C-O_a}=1.217 Å, d_{C-O_b}=1.350 Å, $\angle O_a-C-O_b$=122.72°, $d_{O_b-H_b}$=0.993 Å, d_{C-H_a}=1.106 Å, d_{H_b-N}=2.412 Å, d_{H_a-B}=3.056 Å.

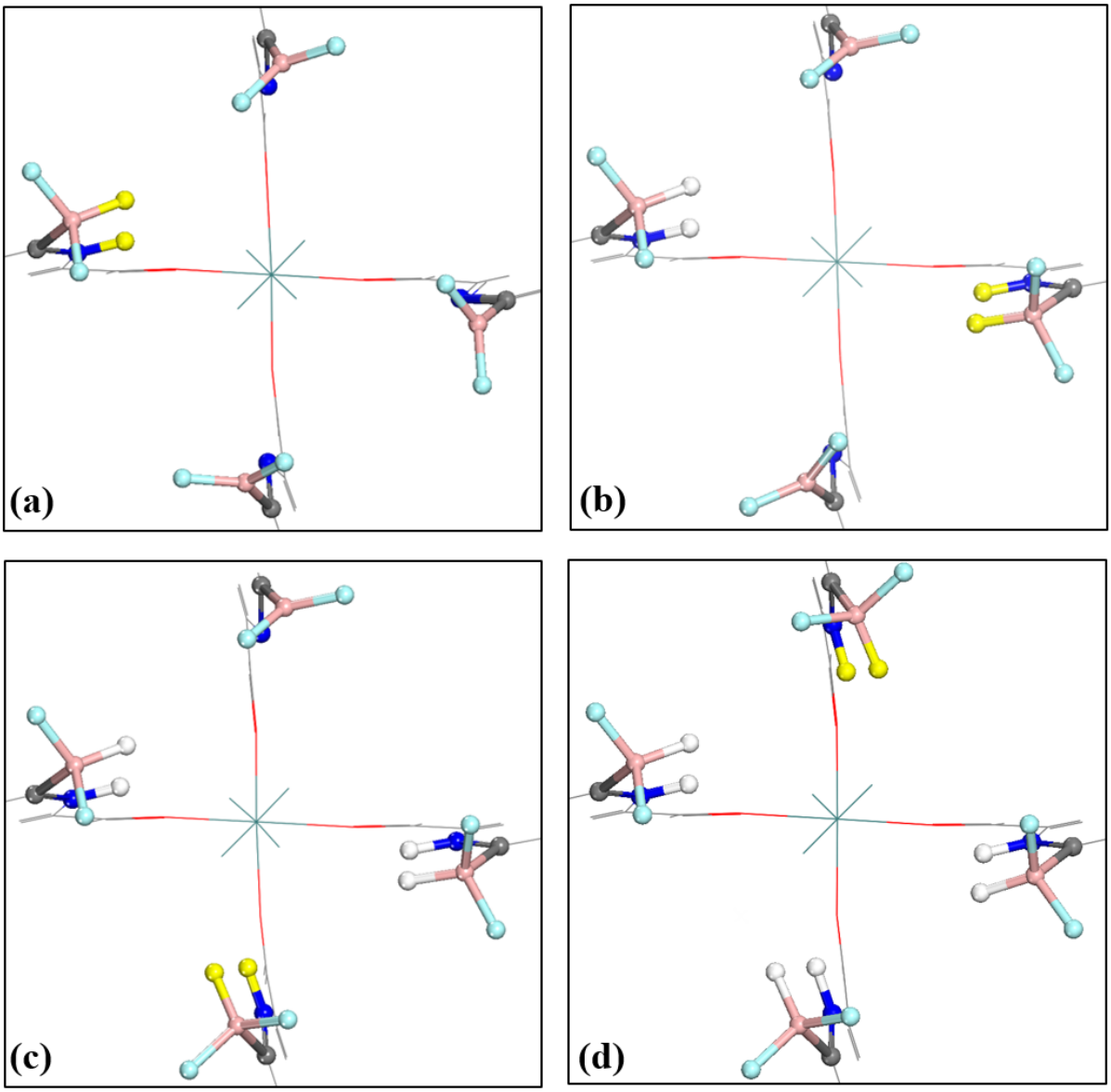

Fig. S5 The top view of sequential H_2 addition in UiO-67-$(NBF_2)_4$ corresponding to Fig. 4.

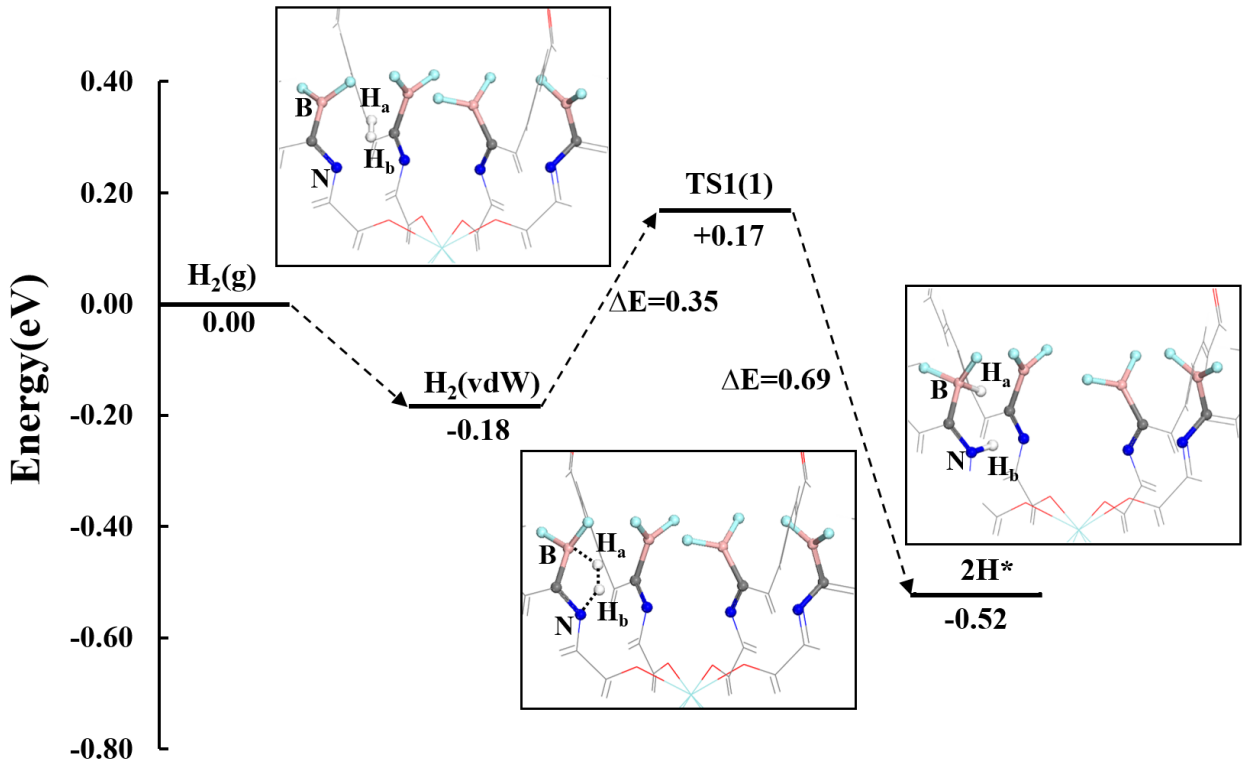

Fig. S6 Potential energy profile for the dissociation of the first H_2 in UiO-67-$(NBF_2)_4$. Structural details of H_2(vdW): $d_{H_a-H_b}$ =0.738 Å, d_{H_a-B} =2.729 Å, d_{H_b-N} =2.476 Å; TS1(1): $d_{H_a-H_b}$ =0.952 Å, d_{H_a-B} =1.465 Å, d_{H_b-N} =1.413 Å; 2H*: $d_{H_a-H_b}$ =2.056 Å, d_{H_a-B} =1.229 Å, d_{H_b-N} =1.032 Å.

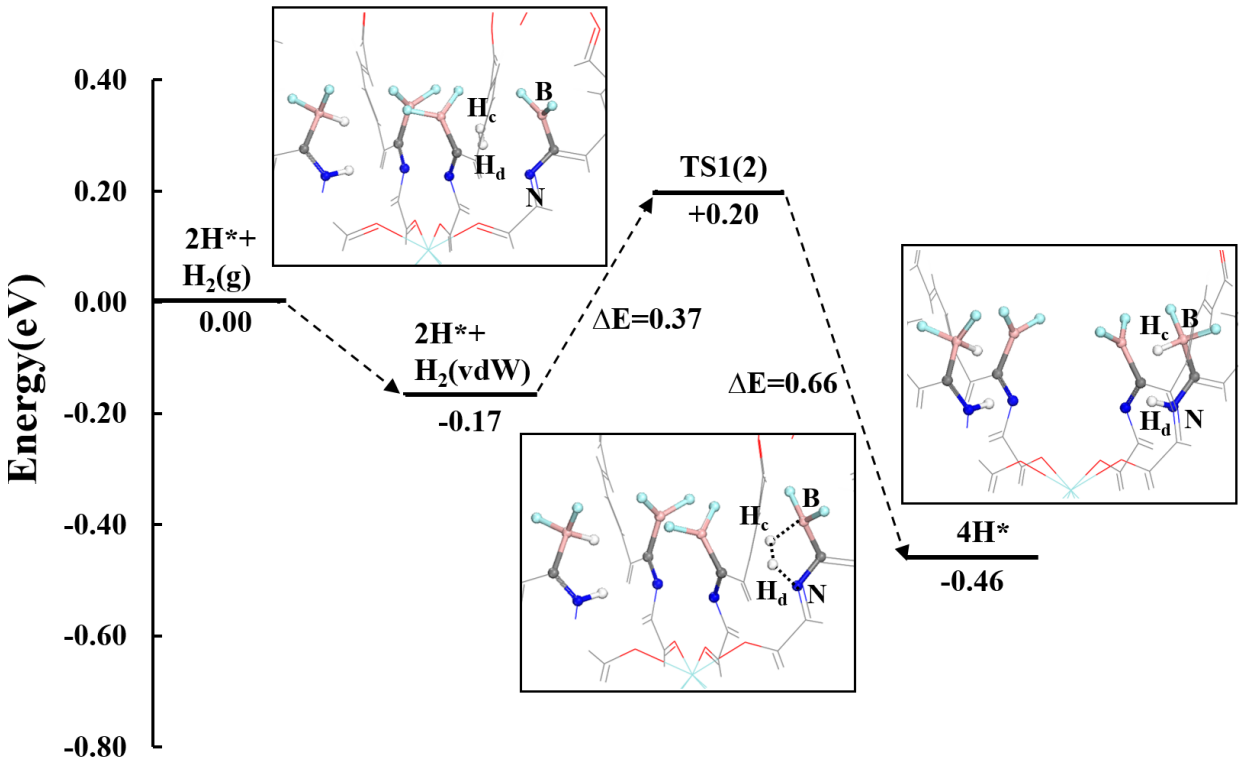

Fig. S7 Potential energy profile for the dissociation of the second H_2 in UiO-67-$(NBF_2)_4$. Structural details of 2H*+H_2(vdW): $d_{H_c-H_d}$ =0.735 Å, d_{H_c-B} =2.833 Å, d_{H_d-N} =2.665 Å; TS1(2): $d_{H_c-H_d}$ =0.946 Å, d_{H_c-B} =1.475 Å, d_{H_b-N} =1.421 Å; 4H*: $d_{H_c-H_d}$ =1.961 Å, d_{H_c-B} =1.231 Å, d_{H_b-N} =1.033 Å.

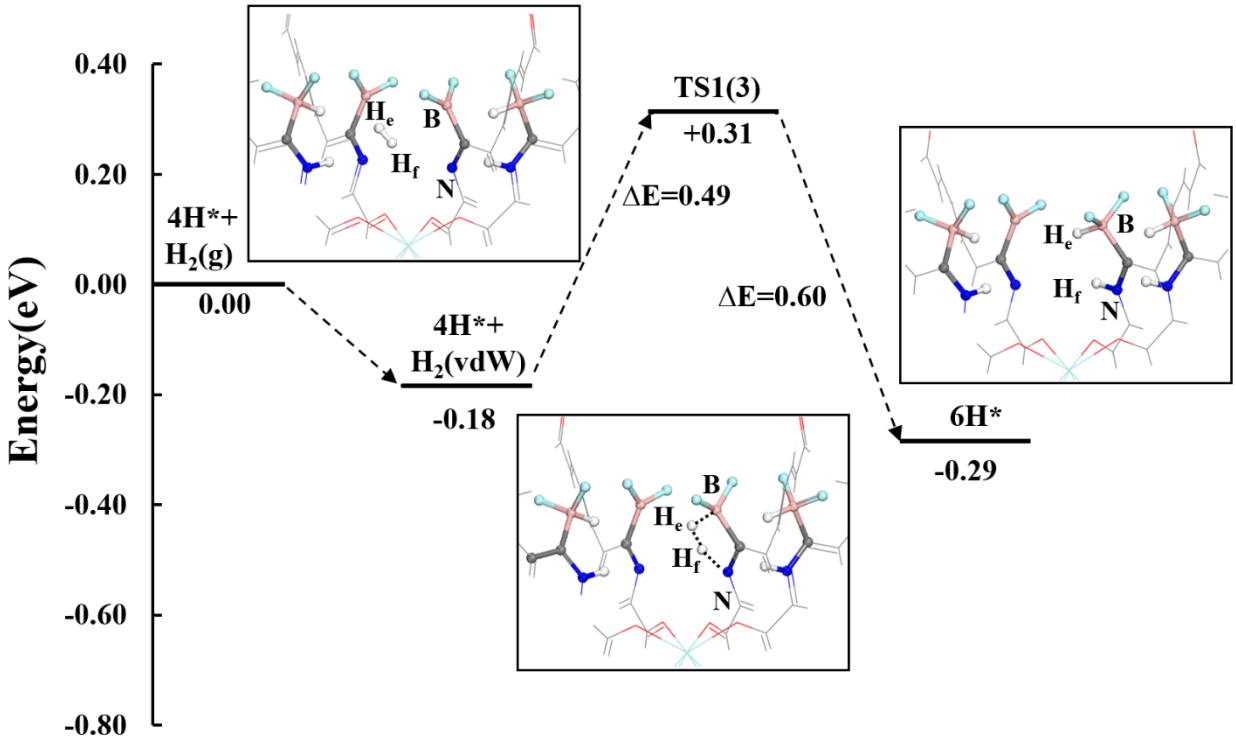

Fig. S8 Potential energy profile for the dissociation of the third H_2 in UiO-67-$(NBF_2)_4$. Structural details of 4H*+H_2(vdW): $d_{H_e-H_f}$ =0.733 Å, d_{H_e-B} =3.645 Å, d_{H_f-N} =2.876 Å; TS1(3): $d_{H_e-H_f}$ =0.981 Å, d_{H_e-B} =1.451 Å, d_{H_f-N} =1.373 Å; 6H*: $d_{H_e-H_f}$ =2.027 Å, d_{H_e-B} =1.231 Å, d_{H_f-N} =1.031 Å.

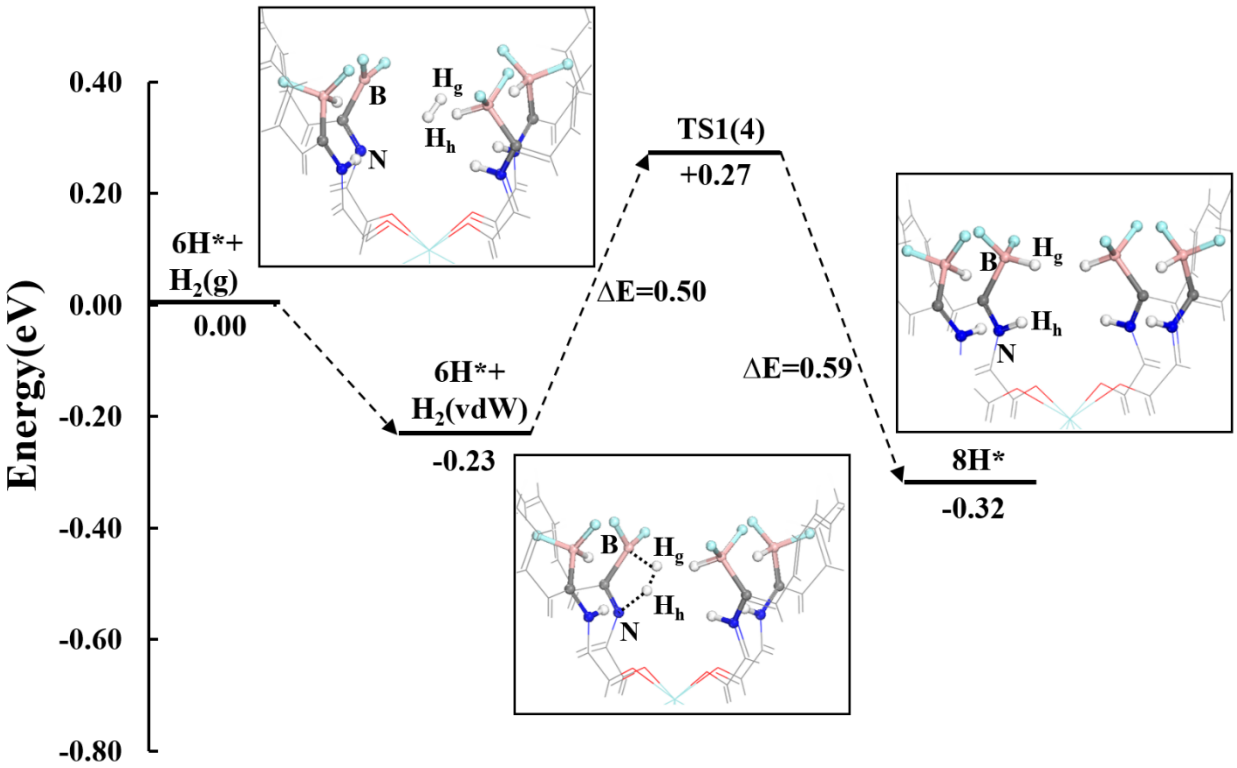

Fig. S9 Potential energy profile for the dissociation of the fourth H_2 in UiO-67-$(NBF_2)_4$. Structural details of 6H*+H_2(vdW): $d_{H_e-H_f}$ =0.738 Å, d_{H_e-B} =2.863 Å, d_{H_f-N} =2.632 Å; TS1(4): $d_{H_e-H_f}$ =0.970 Å, d_{H_e-B} =1.456 Å, d_{H_f-N} =1.382 Å; 8H*: $d_{H_e-H_f}$ =2.020 Å, d_{H_e-B} =1.231 Å, d_{H_f-N} =1.031 Å.

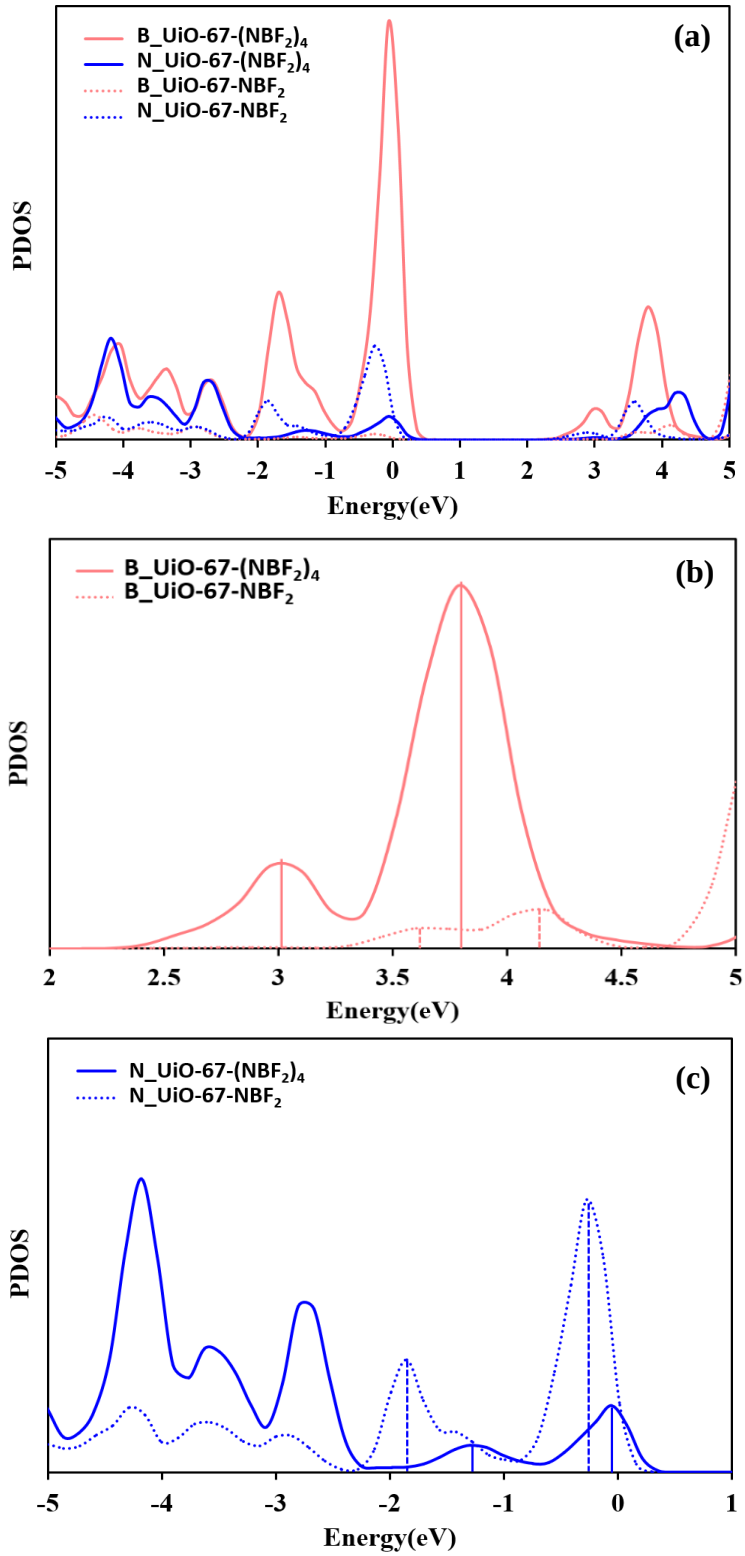

Fig. S10 Projected density of states (PDOS) for B and N atoms in UiO-67-$(NBF_2)_4$ and UiO-67-NBF_2. (a) Plot of both B and N PDOS over both the valence and conduction bands. (b) Conduction band B PDOS. (c) Valence band N PDOS. The Fermi level is normalized at 0 eV in

each graph. The smeared PDOS data were obtained by post-processing using the python code written by Juan Garcia in N. Aaron Deskins's group.[20]

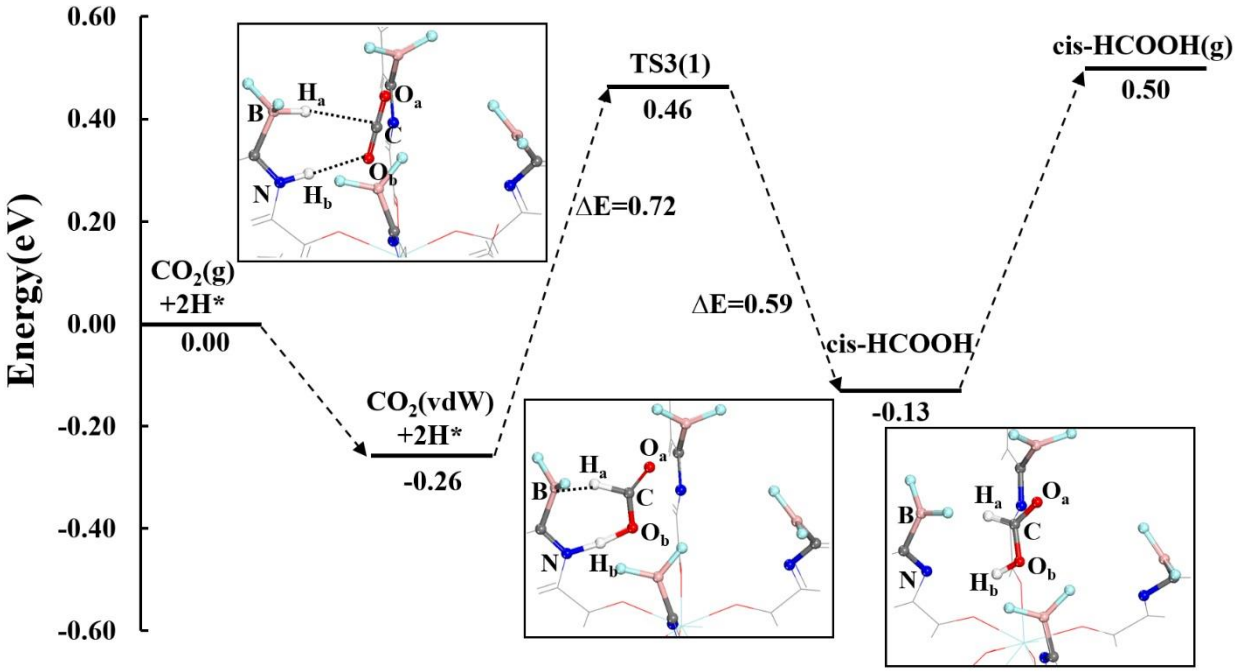

Fig. S11 Potential energy profile for CO_2 reacting with a hydride (H_a) and proton (H_b) in UiO-67-$(NBF_2)_4$ with 2H* (single dissociated H_2). Structural details of CO_2+2H*: d_{C-O_a} =1.173 Å, d_{C-O_b} =1.178 Å, $\angle O_a - C - O_b$ =179.10°, $d_{O_b-H_b}$ =2.147 Å, d_{C-H_a} =2.569 Å, d_{H_b-N} =1.034 Å, d_{H_a-B} =1.224 Å; TS3(1): d_{C-O_a} =1.207 Å, d_{C-O_b} =1.265 Å, $\angle O_a - C - O_b$ =136.41°, $d_{O_b-H_b}$ =1.268 Å, d_{C-H_a} =1.248 Å, d_{H_b-N} =1.238 Å, d_{H_a-B} =1.515 Å; cis-HCOOH: d_{C-O_a} =1.216 Å, d_{C-O_b} =1.350 Å, $\angle O_a - C - O_b$ =122.98°, $d_{O_b-H_b}$ =0.987 Å, d_{C-H_a} =1.106 Å, d_{H_b-N} =2.552 Å, d_{H_a-B} =3.045 Å.

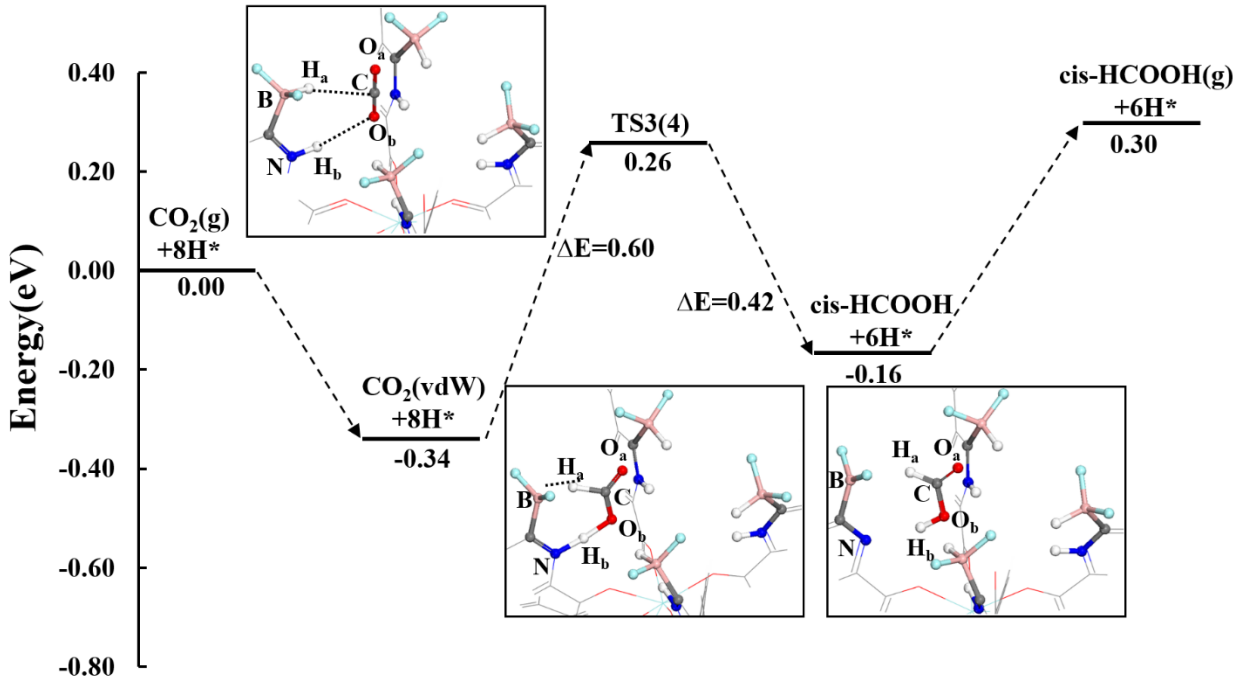

Fig. S12 Potential energy profile for CO_2 reacting with a hydride (H_a) and proton (H_b) in UiO-67-$(NBF_2)_4$ with 8H* (4 dissociated H_2). Structural details of CO_2+2H*: d_{C-O_a} =1.166 Å, d_{C-O_b} =1.187 Å, $\angle O_a-C-O_b$ =178.93°, $d_{O_b-H_b}$ =2.420 Å, d_{C-H_a} =2.519 Å, d_{H_b-N} =1.032 Å, d_{H_a-B} =1.225 Å; TS3(4): d_{C-O_a} =1.203 Å, d_{C-O_b} =1.283 Å, $\angle O_a-C-O_b$ =135.68°, $d_{O_b-H_b}$ =1.305 Å, d_{C-H_a} =1.247 Å, d_{H_b-N} =1.239 Å, d_{H_a-B} =1.555 Å; cis-HCOOH: d_{C-O_a} =1.204 Å, d_{C-O_b} =1.368 Å, $\angle O_a-C-O_b$ =123.66°, $d_{O_b-H_b}$ =0.992 Å, d_{C-H_a} =1.109 Å, d_{H_b-N} =2.107 Å, d_{H_a-B} =2.388 Å.

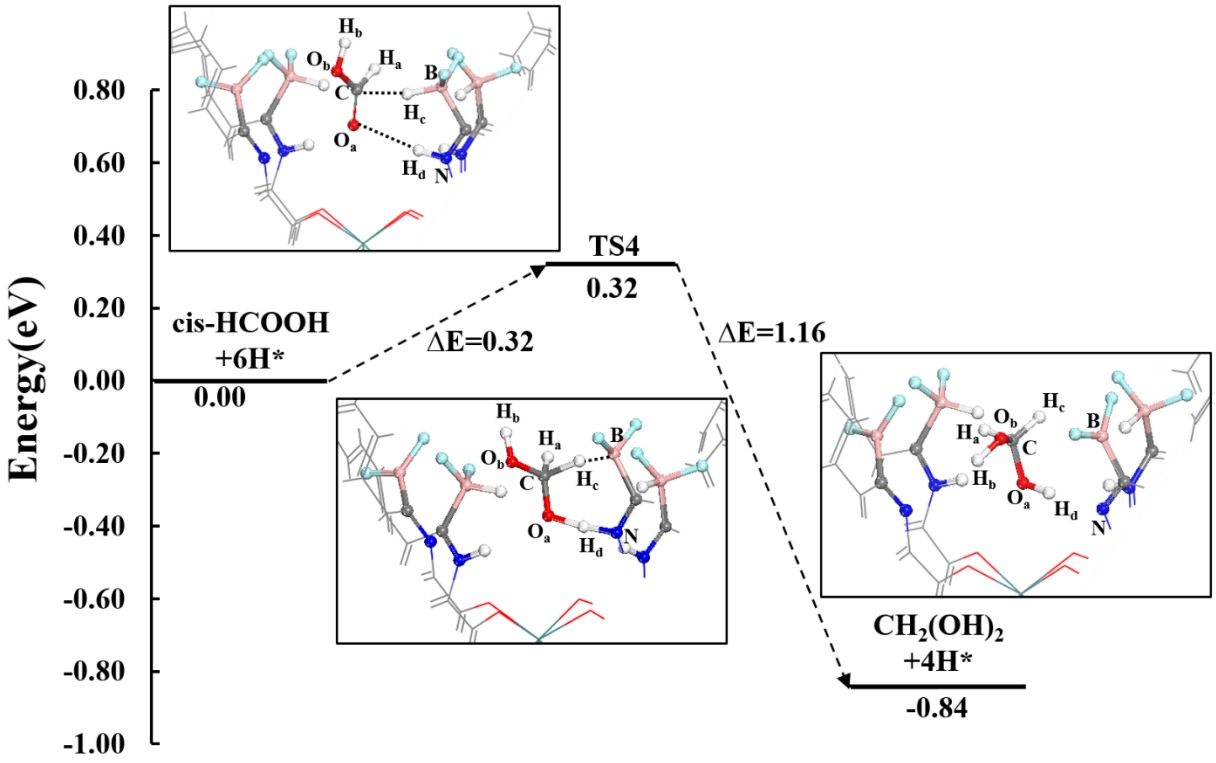

Fig. S13 Potential energy profile for cis-HCOOH reacting with a hydride (H_c) and proton (H_d) in UiO-67-$(NBF_2)_4$ to form methanediol. Structural details of cis-HCOOH+6H*: d_{C-H_c} =2.162 Å, $d_{O_a-H_d}$ =2.403 Å, d_{H_c-B}=1.210 Å, d_{H_d-N} =1.035 Å; TS4: d_{C-H_c} =1.380 Å, $d_{O_a-H_d}$ =1.279 Å, d_{H_c-B} =1.361 Å, d_{H_d-N} =1.224 Å; $CH_2(OH)_2$+4H*: d_{C-H_c} =1.100 Å, $d_{O_a-H_d}$ =0.985 Å, d_{H_c-B}=3.334 Å, d_{H_d-N} =2.119 Å.

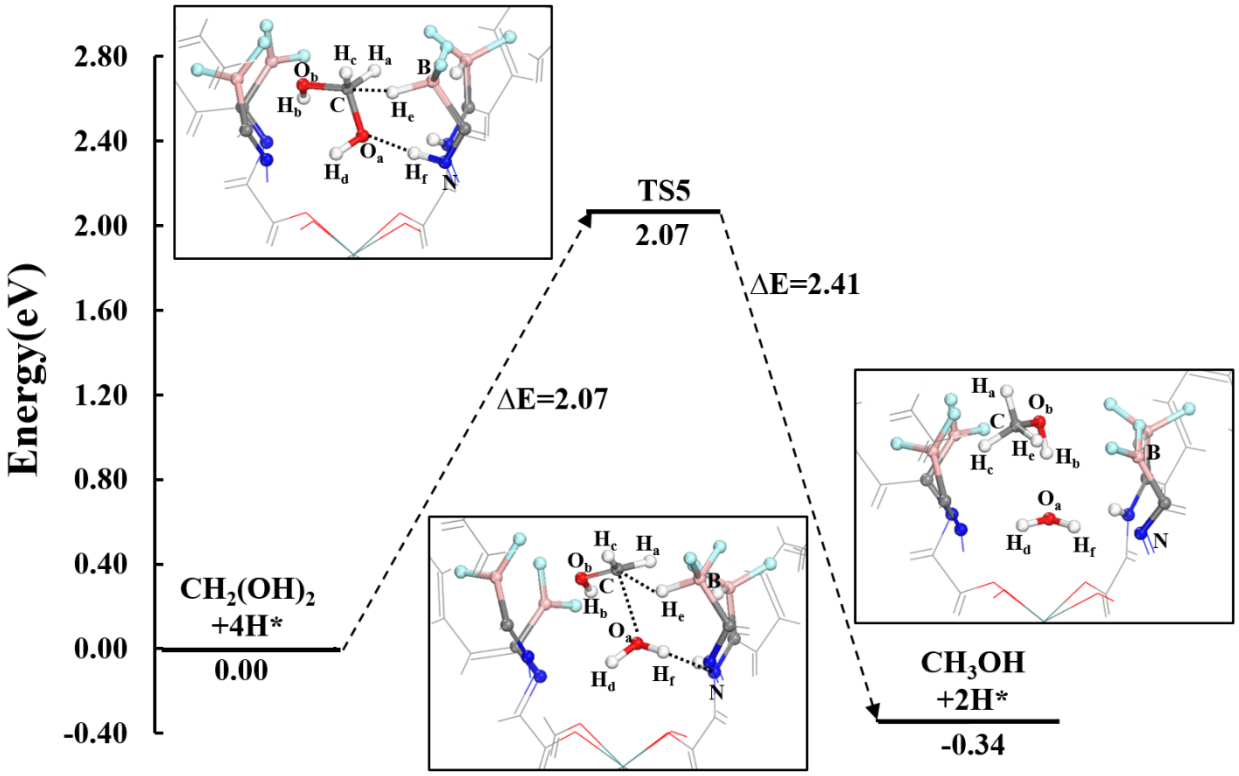

Fig. S14 Potential energy profile for $CH_2(OH)_2$ reacting with a hydride (H_e) and proton (H_f) in UiO-67-$(NBF_2)_4$ to form CH_3OH and H_2O. Structural details of $CH_2(OH)_2$+4H*: d_{C-H_e} =2.806 Å, $d_{O_a-H_f}$ =1.910 Å, d_{H_e-B}=1.221 Å, d_{H_f-N} =1.054 Å; TS5: d_{C-H_e} =2.020 Å, $d_{O_a-H_f}$ =1.013 Å, d_{H_e-B} =1.265 Å, d_{H_f-N} =1.847 Å, d_{C-O_a} =2.298 Å; CH_3OH+2H*: d_{C-H_e} =1.109 Å, $d_{O_a-H_f}$ =0.980 Å, d_{H_e-B}=4.927 Å, d_{H_f-N} =2.724 Å.

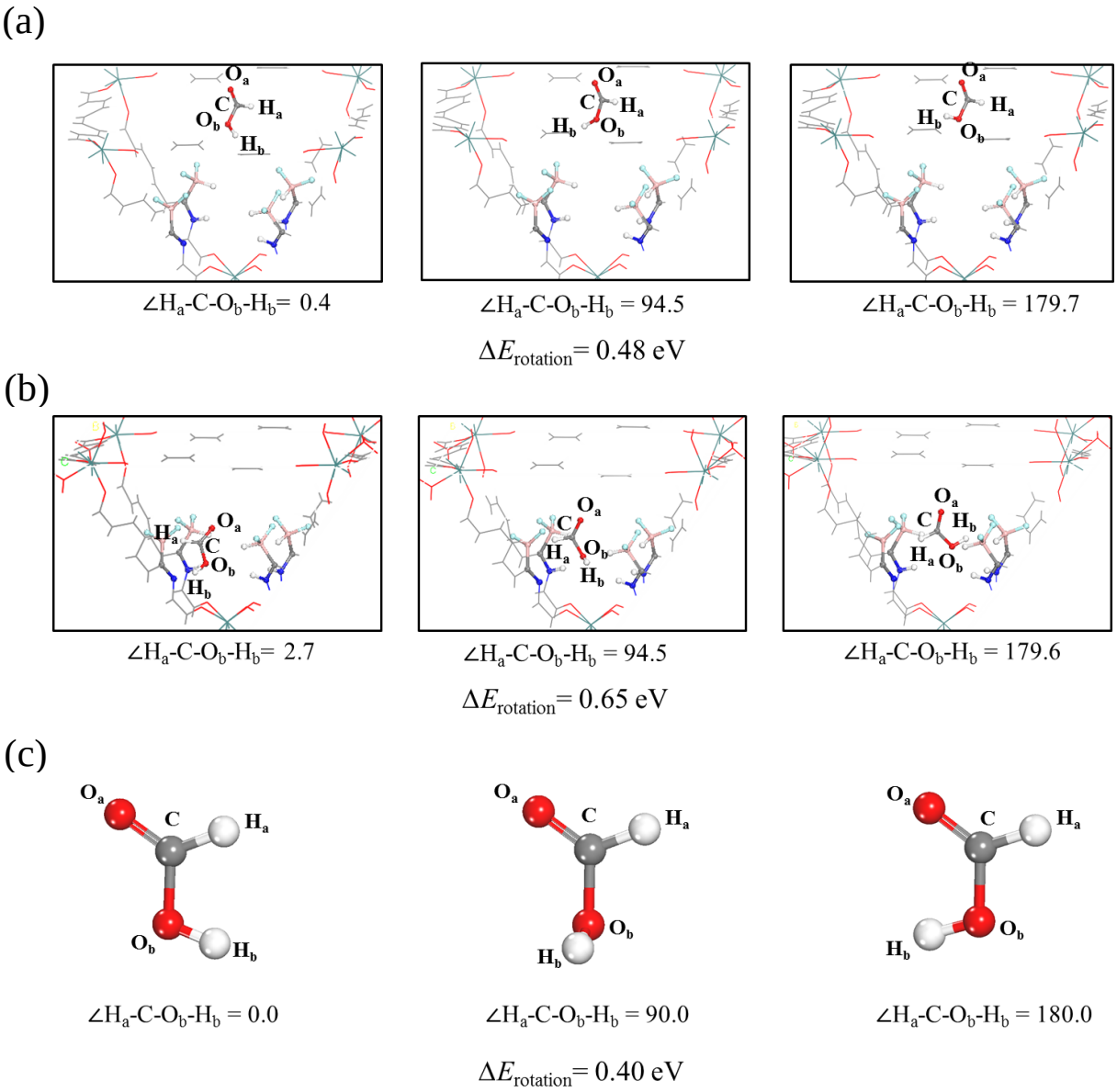

Fig. S15 (a) Potential energy profile for rotation of cis-HCOOH to trans-HCOOH in the center of UiO-67-NBF_2. The torsion angle of H_a-C-O_a-H_b in cis-HCOOH, TS6 and trans-HCOOH are 0.4°, 94.5° and 179.7°, respectively. The rotation barrier is 0.48 eV. (b) The structural details for rotation of cis-HCOOH to trans-HCOOH at the corner of UiO-67-NBF_2. The torsion angle of H_b-C-O_a-H_a in cis-HCOOH, TS and trans-HCOOH are 2.7°, 94.5° and 179.6°, respectively. The rotation barrier is 0.65 eV. The diffusion of cis-HCOOH from the corner to the center of the pore is endothermic by 0.26 eV. (c) The structural details for rotation of cis-HCOOH to trans-HCOOH in the gas phase. The torsion angle of H_b-C-O_a-H_a in cis-HCOOH, TS and trans-HCOOH are 0.0°, 90.0° and 180.0°, respectively. The rotation barrier is 0.40 eV.

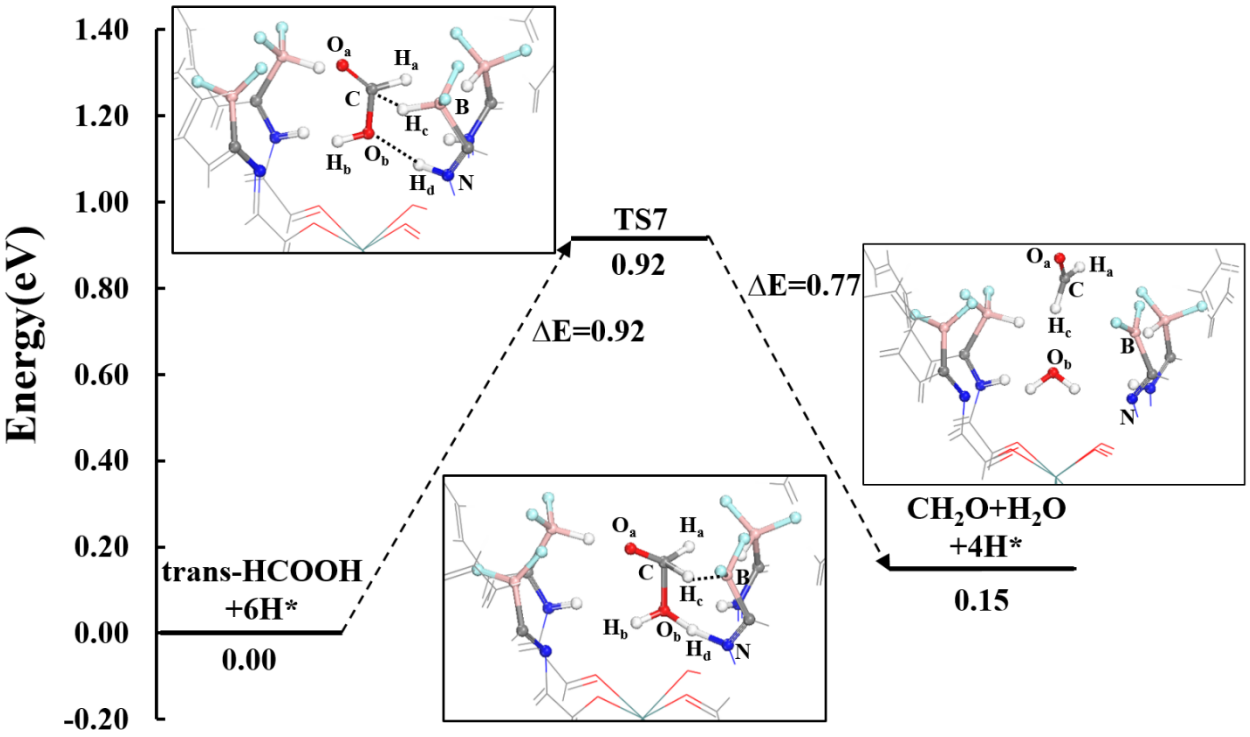

Fig. S16 Potential energy profile for trans-HCOOH reacting with a hydride (H_c) and proton (H_d) in UiO-67-$(NBF_2)_4$ to form CH_2O and H_2O. Structural details of trans-HCOOH+6H*: d_{C-H_c} =2.644 Å, $d_{O_a-H_d}$ =2.198 Å, d_{H_c-B} =1.223 Å, d_{H_d-N} =1.037 Å; TS7: d_{C-H_c} =1.392 Å, $d_{O_a-H_d}$ =1.198 Å, d_{H_c-B} =1.356 Å, d_{H_d-N} =1.348 Å; CH_2O+H_2O+4H*: d_{C-H_c} =1.109 Å, $d_{O_a-H_d}$ =0.977 Å, d_{H_c-B} =3.709 Å, d_{H_d-N} =2.339 Å.

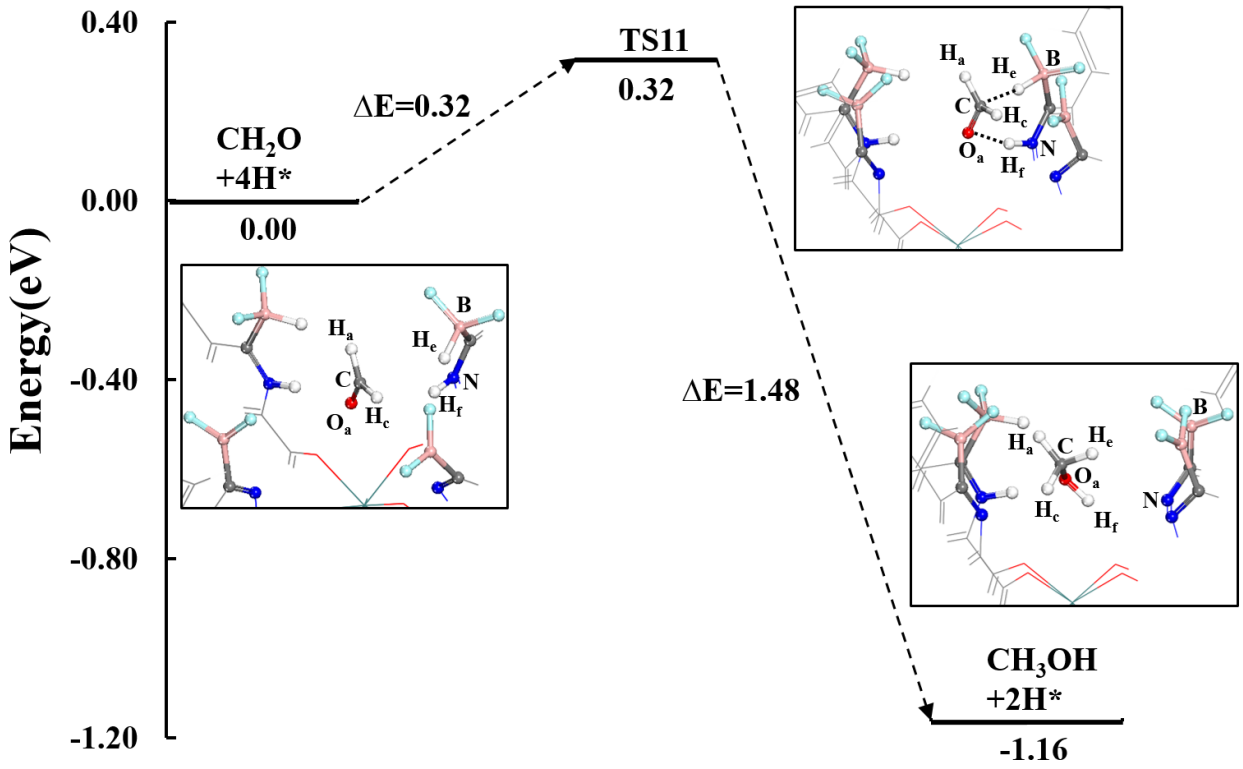

Fig. S17 Potential energy profile for CH_2O reacting with a hydride (H_g) and proton (H_h) in UiO-67-$(NBF_2)_4$. Structural details of CH_2O+4H*: d_{C-H_g} =2.812 Å, d_{H_g-B} =1.235 Å, d_{C-O_a} =1.225 Å, $d_{O_a-H_h}$ =2.763 Å, d_{H_h-N} =1.032 Å; TS11: d_{C-H_g} =1.502 Å, d_{H_g-B} =1.320 Å, d_{C-O_a} =1.276 Å, $d_{O_a-H_h}$ =1.587 Å, d_{H_h-N} =1.086 Å; CH_3OH+2H*: d_{C-H_g} =1.099 Å, d_{H_g-B} =4.043 Å, d_{C-O_a} =1.445 Å, $d_{O_a-H_h}$ =0.978 Å, d_{H_h-N} =2.684 Å.

Table S6. The energy data for Fig. 6.

Species	Energy(eV)
CO_2(g)+4H_2(g)	0.00
CO_2(g)+8H*	-1.59
CO_2+8H*	-1.93
cis-HCOOH+6H*	-1.57
trans-HCOOH+6H*	-1.75
$CH_2(OH)_2$+4H*	-2.41
CH_2O+H_2O+2H*	-2.09
CH_3OH+H_2O+2H*	-2.75
CH_3OH(g)+H_2O(g)+2H*	-2.00
TS3(4)	-1.33
TS4	-1.25
TS5	-0.34
TS6	-1.13
TS7	-0.83
TS8	-0.62
TS9	-1.39
TS10	-1.82
TS11	-1.67

Table S7. The forward reaction energies ΔE_r (eV) and barriers ΔE_b (eV) for the elementary reactions involving methanol production in UiO-67-$(NBF_2)_4$.

reactions	ΔE_r	ΔE_b
H_2→2H*	-0.52	0.35
H_2+2H*→4H*	-0.46	0.37
H_2+4H*→6H*	-0.29	0.49
H_2+6H*→8H*	-0.32	0.50
CO_2+8H*→cis-HCOOH+6H*	0.18	0.60
cis-HCOOH+6H*→$CH_2(OH)_2$+4H*	-0.84	0.32
$CH_2(OH)_2$+4H*→CH_3OH+H_2O+2H*	-0.34	2.07
cis-HCOOH→trans-HCOOH	-0.18	0.44
trans-HCOOH+6H*→CH_2O+H_2O+4H*	0.15	0.92
$CH_2(OH)_2$+4H*→ CH_2O+H_2O+4H*	0.32	1.79
$CH_2(OH)_2$+4H*+H_2O→ CH_2O+2H_2O+4H*	0.43	1.02
$CH_2(OH)_2$+4H*+HCOOH→CH_2O+H_2O+4H*+HCOOH	0.45	0.59
CH_2O+4H*→CH_3OH+2H*	-1.16	0.32
CH_3OH+H_2O+2H*→ CH_3OH+H_2O(g)+2H*	0.13	-
CH_3OH+2H*→ CH_3OH(g)+2H*	0.62	-

Table S8. Structural details for Fig. 7-11.

Fig. 7	$CH_2(OH)_2$+4H*	TS8	CH_2O+H_2O+4H*
	d_{C-O_a} =1.439 Å	d_{C-O_a} =1.331 Å	d_{C-O_a} =1.225 Å
	$d_{O_a-H_d}$ =0.973 Å	$d_{O_a-H_d}$ =1.357 Å	$d_{O_a-H_d}$ =3.386 Å
	$d_{H_d-O_b}$ =2.488 Å	$d_{H_d-O_b}$ =1.184 Å	$d_{H_d-O_b}$ =0.977 Å
Fig. 8	$CH_2(OH)_2$+ H_2O+4H*	TS9	CH_2O+H_2O+ H_2O+4H*
	d_{C-O_b} =1.453	d_{C-O_b} =1.785 Å	d_{C-O_b} =2.542 Å
	$d_{O_b-H_j}$ =1.969 Å	$d_{O_b-H_j}$ =1.201 Å	$d_{O_b-H_j}$ =0.991 Å
	$d_{H_j-O_i}$ =0.982 Å	$d_{H_j-O_i}$ =1.261 Å	$d_{H_j-O_i}$ =1.830Å
	$d_{O_a-H_d}$ =0.987 Å	$d_{O_a-H_d}$ =1.302 Å	$d_{O_a-H_d}$ =1.935 Å
	$d_{H_d-O_i}$ =1.929 Å	$d_{H_d-O_i}$ =1.163 Å	$d_{H_d-O_i}$ =0.985 Å
Fig. 9	$CH_2(OH)_2$+HCOOH+4H*	TS10	CH_2O+H_2O+ H_2O+4H*
	$d_{O_j-H_d}$ =1.795 Å	$d_{O_j-H_d}$ =1.178 Å	d_{C-O_b} =2.542 Å
	$d_{H_d-O_a}$ =0.993 Å	$d_{H_d-O_a}$ =1.274 Å	$d_{O_b-H_j}$ =0.991 Å
	$d_{O_i-H_i}$ =1.019 Å	$d_{O_i-H_i}$ =1.424 Å	$d_{H_j-O_i}$ =1.830Å
	$d_{H_i-O_b}$ =1.628 Å	$d_{H_i-O_b}$ =1.075 Å	$d_{O_a-H_d}$ =1.935 Å
	d_{C-O_b} =1.462 Å	d_{C-O_b} =1.828 Å	$d_{H_d-O_i}$ =0.985 Å
Fig. 11	$CH_2(OH)_2$	TS12	CH_2O+H_2O
	d_{C-O_b} =1.467 Å	d_{C-O_b} =1.838 Å	d_{C-O_b} =2.373 Å
	$d_{O_b-H_i}$ =1.741 Å	$d_{O_b-H_i}$ =1.096 Å	$d_{O_b-H_i}$ =0.994 Å
	$d_{O_i-H_i}$ =1.012 Å	$d_{O_i-H_i}$ =1.408 Å	$d_{O_i-H_i}$ =1.792 Å
	d_{C-O_a} =1.391 Å	d_{C-O_a} =1.289 Å	d_{C-O_a} =1.236 Å
	$d_{O_a-H_d}$ =1.992 Å	$d_{O_a-H_d}$ =1.233 Å	$d_{O_a-H_d}$ =1.634 Å
	$d_{H_d-O_j}$ =1.788 Å	$d_{H_d-O_j}$ =1.207 Å	$d_{H_d-O_j}$ =1.020 Å

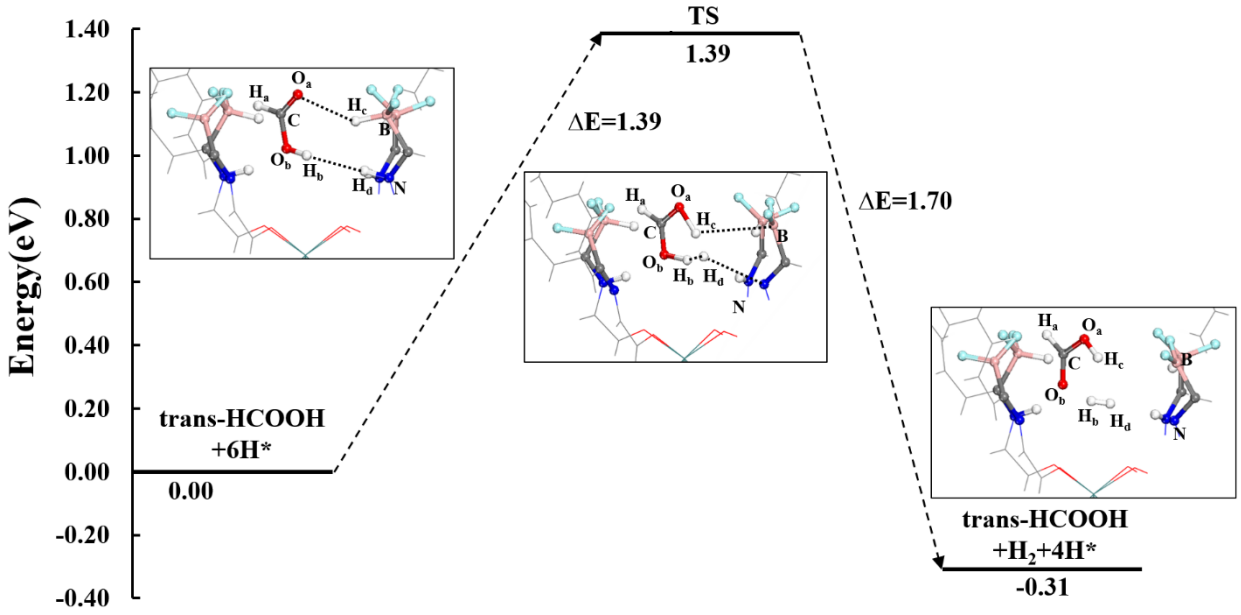

Fig. S18 Potential energy profile for HCOOH reacting with hydride (H_c) and proton (H_d) to produce H_2 in UiO-67-$(NBF_2)_4$. Structural details of trans-HCOOH+6H*: $d_{O_a-H_c}$ =2.899 Å, d_{H_c-B} =1.227 Å, $d_{O_b-H_b}$ =0.988 Å, $d_{H_b-H_d}$ =2.465Å, d_{H_d-N} =1.031 Å; TS12: $d_{O_a-H_c}$ =1.323 Å, d_{H_c-B} =3.413 Å, $d_{O_b-H_b}$ =1.324 Å, $d_{H_b-H_d}$ =0.998 Å, d_{H_d-N} =2.721 Å; trans-HCOOH+H_2+4H*: $d_{O_a-H_c}$ =0.984 Å, d_{H_c-B} =3.793 Å, $d_{O_b-H_b}$ =2.963 Å, $d_{H_b-H_d}$ =0.739 Å, d_{H_d-N} =2.622 Å.

Table S9. Comparison of the forward reaction energies ΔE_r (eV) and barriers ΔE_b (eV) for $CH_2(OH)_2 \rightarrow CH_2O$ in UiO-67-NBF_2 and gas phase.

	$CH_2(OH)_2 - CH_2O+H_2O$		$CH_2(OH)_2 \xrightarrow{H_2O} CH_2O+H_2O$		$CH_2(OH)_2 \xrightarrow{HCOOH} CH_2O+H_2O$	
	ΔE_r	ΔE_b	ΔE_r	ΔE_b	ΔE_r	ΔE_b
UiO-67-NBF_2	0.32	1.79	0.43	1.02	0.45	0.59
Gas phase	0.51	1.84	0.42	1.01	0.46	0.62
Gas phase [a]	0.38	2.06	0.32	1.27	0.45	0.80
Gas phase [b]	0.34	2.06	0.29	1.30	0.40	0.82
Gas phase [c]	0.37	2.09	0.36	1.39	0.46	0.92

Note: The gas phase results are obtained from Harza et al.[21] calculated using Gaussian 03 and 09 at different levels of theory: [a] B3LYP/ 6-31+G(d,p), [b] B3LYP/ 6-311++G(3df,3pd), [c] MP2/6-311++G(3df,3pd).

Table S10. The binding energies (eV) for different molecules in UiO-67-$(NBF_2)_4$. n represent the number of H_2 chemisorbed in UiO-67-$(NBF_2)_4$. CO_2, HCOOH, $CH_2(OH)_2$, CH_2O, CH_3OH and H_2O are chemisorbed in UiO-67-$(NBF_2)_4$ when *n*=1, 2, 3, and the structures are shown in Fig. S19, S20 and S21, respectively. When *n*=4, CO_2, HCOOH, $CH_2(OH)_2$, CH_2O, CH_3OH and H_2O are physisorbed, as shown in Fig. S22. cis-HCOOH is physisorbed in the pore for *n*=1 to 4, with a geometry similar to trans-HCOOH shown in Fig. S22.

Species	n=1	n=2	n=3	n=4
CO_2	-0.30	-0.42	-0.14	-0.03
cis-HCOOH	-0.12	-0.15	-0.07	-0.23
trans-HCOOH	-0.49	-0.70	-0.83	-0.30
$CH_2(OH)_2$	-1.06	-1.22	-1.34	-0.08
CH_2O	-1.84	-1.60	-1.55	-0.21
CH_3OH	-1.06	-0.97	-1.00	-0.12
H_2O	-1.03	-1.00	-0.97	-0.11

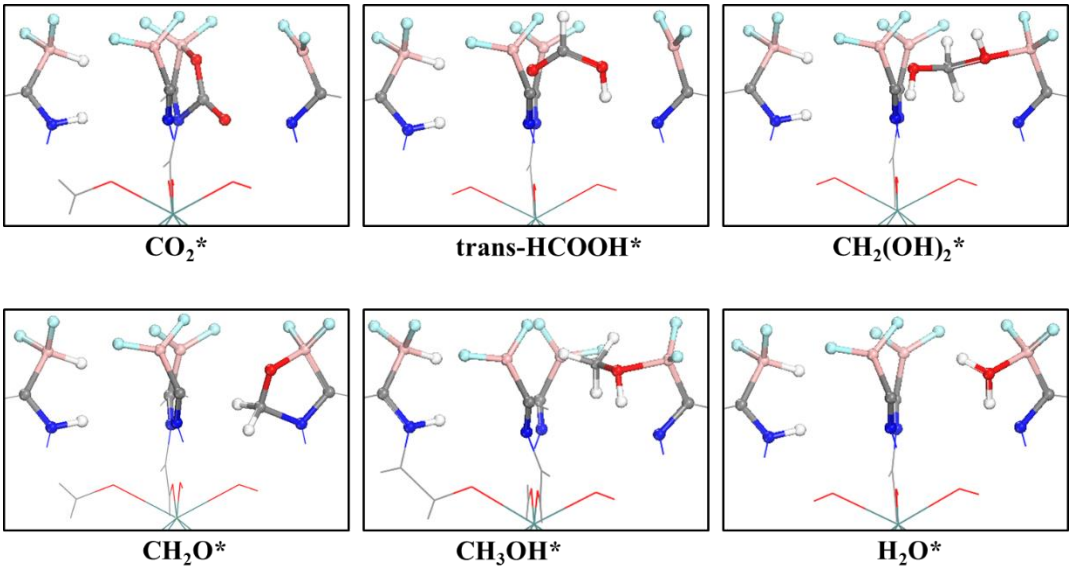

Fig. S19 The structures of CO_2*, trans-HCOOH*, $CH_2(OH)_2$*, CH_2O*, CH_3OH*, H_2O* chemisorbed in UiO-67-$(NBF_2)_4$ with one chemisorbed H_2.

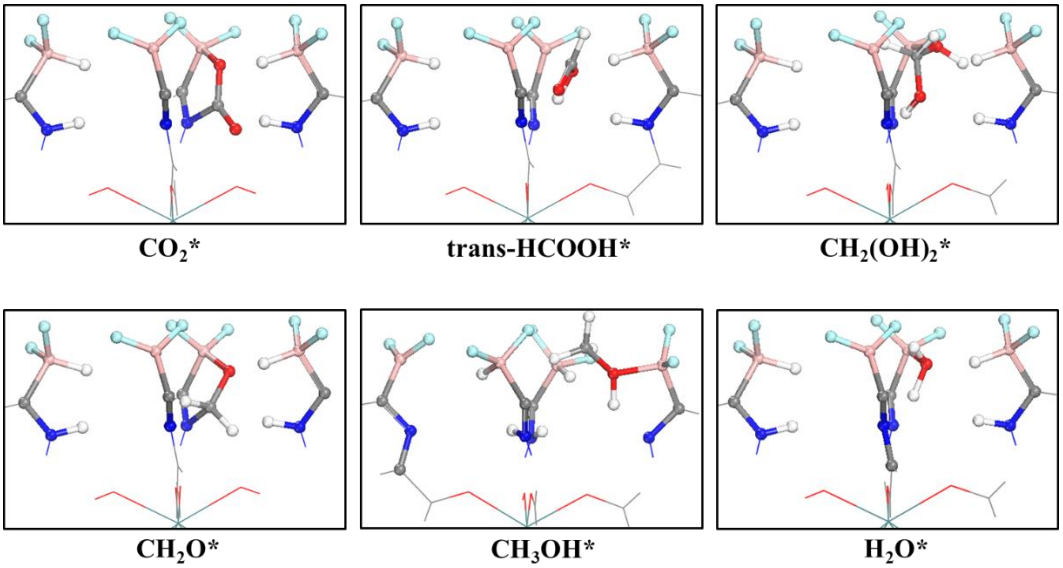

Fig. S20 The structures of CO_2*, trans-HCOOH*, $CH_2(OH)_2$*, CH_2O*, CH_3OH*, H_2O* chemisorbed in UiO-67-$(NBF_2)_4$ with two chemisorbed H_2.

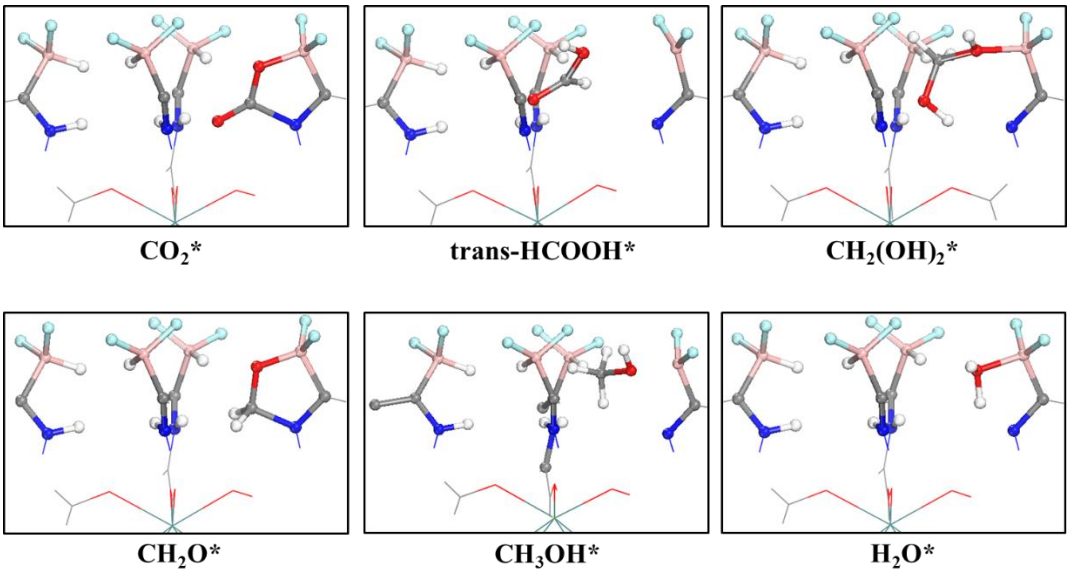

Fig. S21 The structures of CO_2*, trans-HCOOH*, $CH_2(OH)_2$*, CH_2O*, CH_3OH*, H_2O* chemisorbed in UiO-67-$(NBF_2)_4$ chemisorbed with three H_2.

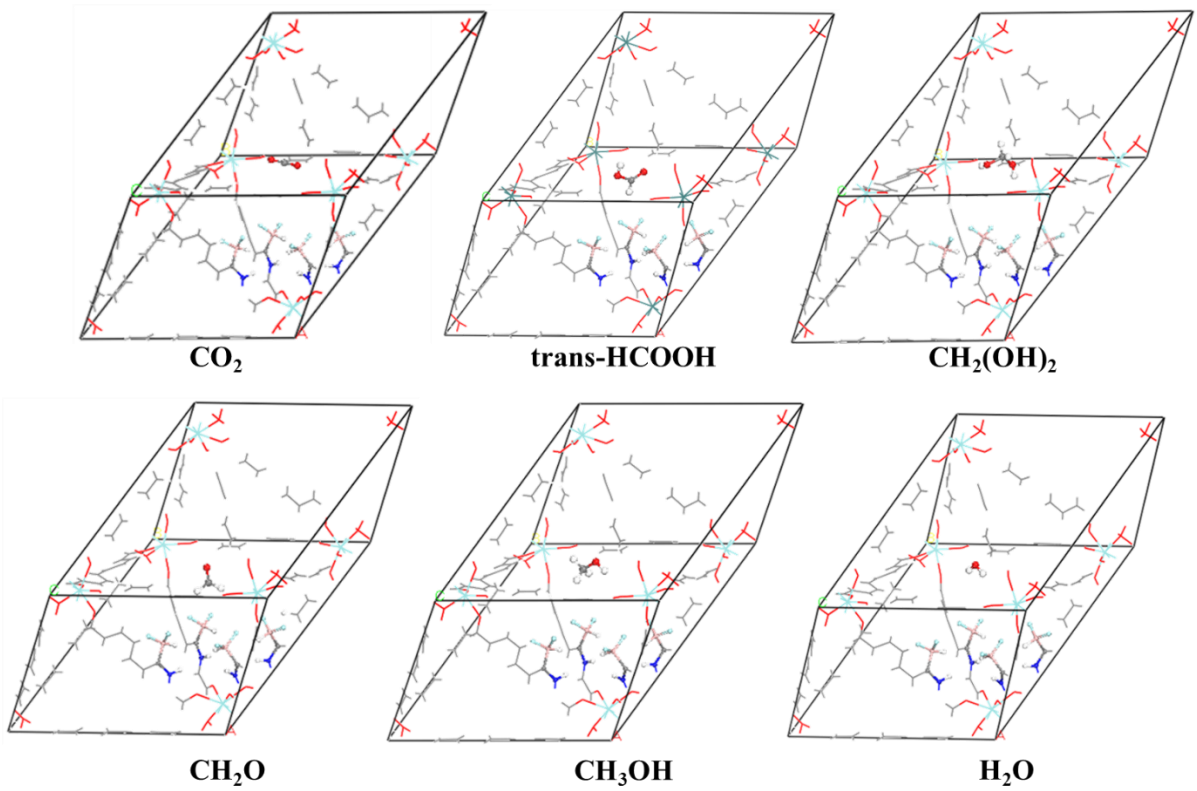

Fig. S22 The structures of CO_2, trans-HCOOH, $CH_2(OH)_2$, CH_2O, CH_3OH and H_2O physisorbed in UiO-67-$(NBF_2)_4$ with four chemisorbed H_2.

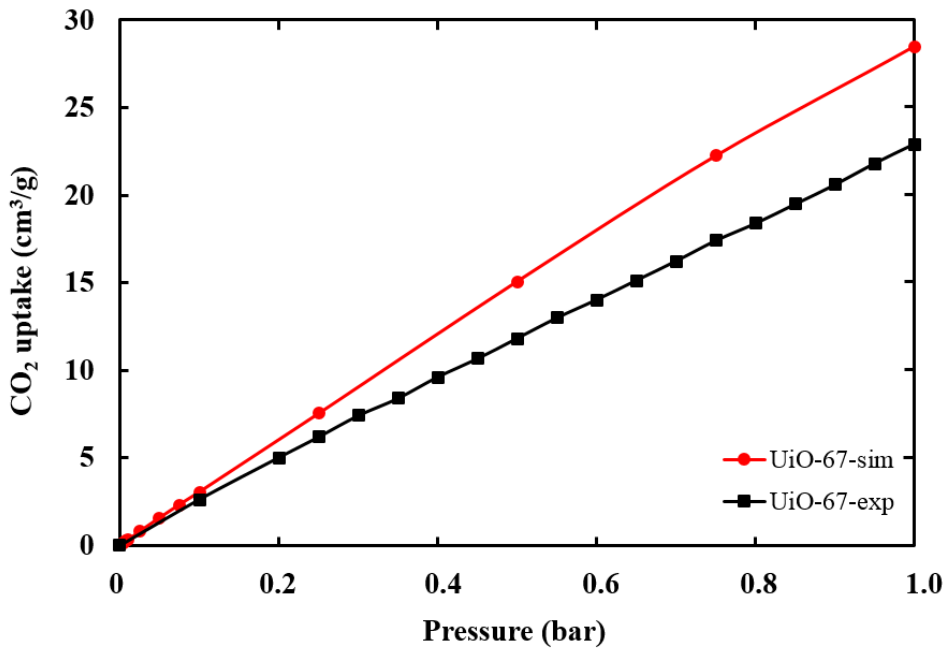

Fig. S23 Comparison between experimental[22] and simulated CO_2 adsorption isotherms in UiO-67 at 298 K. Lines are drawn as a guide to the eye. The simulated isotherm is larger than experiments, which is to be expected for sorbent materials having some fraction of blocked pores from defects or incomplete activation.

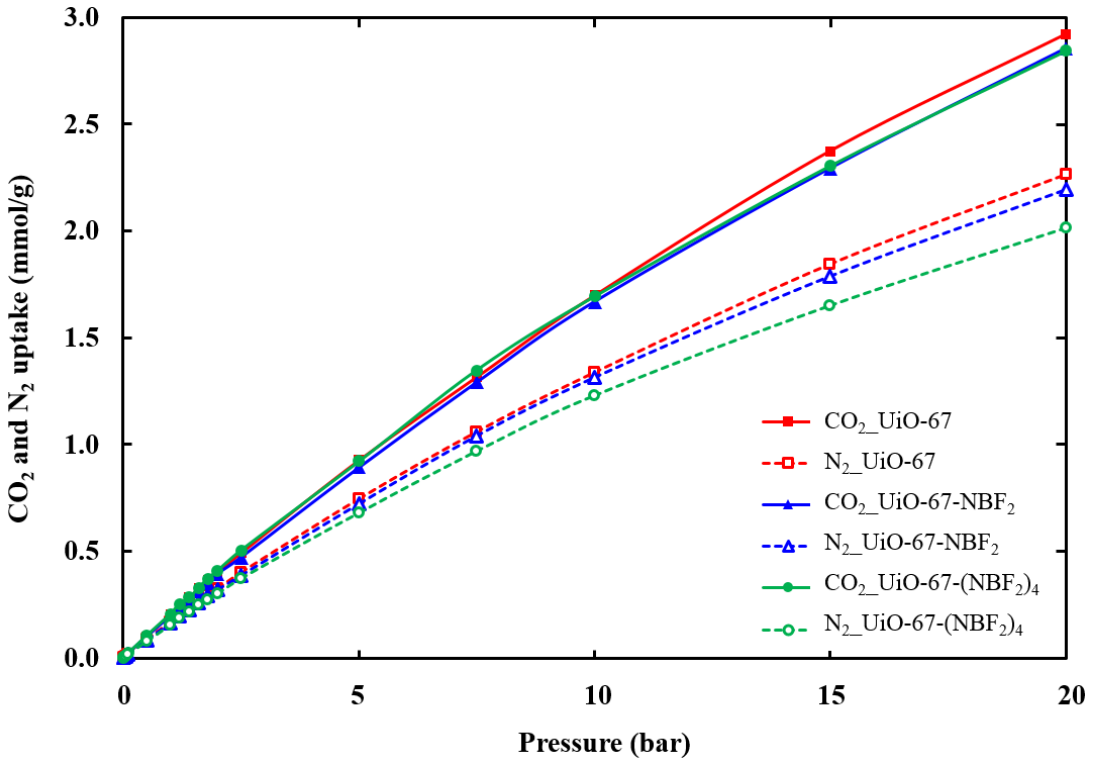

Fig. S24 The simulated CO_2 and N_2 adsorption isotherms for a 15:85 CO_2/N_2 mixture in UiO-67, UiO-67-NBF_2 and UiO-67-$(NBF_2)_4$ at 298K. Lines are drawn as a guide to the eye.

Microkinetic modeling of adsorption-desorption of H_2 and CO_2

Equations (1) and (2) described the adsorption of H_2 and CO_2 in UiO-67-NBF_2:

$$\mathrm{H_2(vdW)} + * \rightleftharpoons 2\mathrm{H}* \tag{1}$$

$$\mathrm{CO_2(vdW)} + * \rightleftharpoons \mathrm{CO_2}* \tag{2}$$

The * symbol in the equations above denotes the Lewis pair (LP) acid and base sites, so that one * can accommodate both dissociated H atoms in eq(1). We assume that adsorption/desorption of H_2 and CO_2 is in equilibrium, giving

$$\vec{k}_1 C_{\mathrm{H_2}} \theta* = \overleftarrow{k}_1 \theta_{2\mathrm{H}*} \tag{3}$$

$$\vec{k}_2 C_{\mathrm{CO_2}} \theta* = \overleftarrow{k}_2 \theta_{\mathrm{CO_2}*} \tag{4}$$

The equilibrium adsorption constant for H_2 and CO_2 are given by

$$K_1 = \frac{\theta_{2\mathrm{H}*}}{C_{\mathrm{H_2}} \theta*} \tag{5}$$

$$K_2 = \frac{\theta_{\mathrm{CO_2}*}}{C_{\mathrm{H_2}} \theta*} \tag{6}$$

The total coverage is $\theta* + \theta_{2H*} + \theta_{CO_2*} = 1$, where

$$\theta* = \frac{1}{1 + K_1 C_{H_2} + K_2 C_{CO_2}} \tag{7}$$

$$\theta_{2H*} = \frac{K_1 C_{H_2}}{1 + K_1 C_{H_2} + K_2 C_{CO_2}} \tag{8}$$

$$\theta_{CO_2*} = \frac{K_2 C_{\mathrm{CO_2}}}{1 + K_1 C_{\mathrm{H_2}} + K_2 C_{\mathrm{CO_2}}} \tag{9}$$

The coverage ratio of H_2 and CO_2 is therefore given by

$$\frac{\theta_{2H*}}{\theta_{CO_2*}} = \frac{K_1 C_{H_2}}{K_2 C_{CO_2}} \tag{10}$$

The adsorption equilibrium constants of eq(5) and eq(6) are given by

$$K_1 = \exp\left(\frac{-\left(\Delta E_1 - \mathrm{T}\Delta S_1\right)}{k_{\mathrm{B}} \mathrm{T}} \right) \tag{11}$$

$$K_2 = \exp\left(\frac{-\left(\Delta E_2 - \mathrm{T}\Delta S_2\right)}{k_\mathrm{B}\mathrm{T}}\right) \tag{12}$$

We assume that the difference in entropy between the physisorbed and chemisorbed species in UiO-67-NBF_2 is small because of the highly confined nature of the physisorbed molecules in UiO-67-NBF_2, which allows only hindered rotations and little translational freedom. Hence, we assume that $\left|T\Delta S_i\right| \ll \left|\Delta E_i\right|$ for i = 1, 2. Hence,

$$K_1 = \exp\left(\frac{-\Delta E_1}{k_\mathrm{B}\mathrm{T}}\right) \tag{13}$$

$$K_2 = \exp\left(\frac{-\Delta E_2}{k_\mathrm{B}\mathrm{T}}\right) \tag{14}$$

As a result,

$$\frac{\theta_{2H^*}}{\theta_{CO_2^*}} = \frac{C_{\mathrm{H}_2}\exp\left(-\Delta E_1 / k_B\mathrm{T}\right)}{C_{\mathrm{CO}_2}\exp\left(-\Delta E_2 / k_B\mathrm{T}\right)} = \frac{C_{\mathrm{H}_2}}{C_{\mathrm{CO}_2}}\exp\left(\frac{-\Delta E_1 + \Delta E_2}{k_B\mathrm{T}}\right) = \frac{C_{\mathrm{H}_2}}{C_{\mathrm{CO}_2}}\exp\left(\frac{0.26}{k_B\mathrm{T}}\right) \tag{15}$$

We summarize the ratio of 2H* and CO_2* ($\theta_{2\mathrm{H}^*} / \theta_{\mathrm{CO}_2^*}$) in UiO-67-$NBF_2$ in Table S11.

Table S11 The ratio of 2H* and CO_2* ($\theta_{2\mathrm{H}^*} / \theta_{\mathrm{CO}_2^*}$) in UiO-67-$NBF_2$ at different temperatures and concentrations of H_2 and CO_2.

$\theta_{2\mathrm{H}^*} / \theta_{\mathrm{CO}_2}$		**T(K)**				
		298	350	400	450	500
$C_{\mathrm{H}_2} / C_{\mathrm{CO}_2}$	3:1	74859	16632	5662	2449	1252
	1:1	24953	5544	1887	816	418
	1:100	250	233	55	8	4

If the UiO-67-NBF_2 is highly selective toward CO_2 over H_2 the sites will still not be poisoned by CO_2 because the ratios in S11 are so large. Hence, if the ratio of concentrations of H_2/CO_2 in the pore is 0.01, the $\theta_{2\mathrm{H}^*} / \theta_{\mathrm{CO}_2^*}$ is still on the order of 100 at 298 K or 350 K.

References

1. C.-J. Zhao, D. Xue, Z.-H. Jia, C. Wang and J. Xiao, *Synlett*, 2014, **25**, 1577-1584.
2. K. Ishihara, K. Inanaga, S. Kondo, M. Funahashi and H. Yamamoto, *Synlett*, 1998, 1053-1056.
3. G. W. Peterson, J. B. DeCoste, F. Fatollahi-Fard and D. K. Britt, *Ind. Eng. Chem. Res.*, 2014, **53**, 701-707.
4. Q. Chen, Q. He, M. Lv, Y. Xu, H. Yang, X. Liu and F. Wei, *Appl. Surf. Sci.*, 2015, **327**, 77-85.
5. K.-Y. A. Lin, Y.-T. Liu and S.-Y. Chen, *J. Colloid Interface Sci.*, 2016, **461**, 79-87.
6. P. M. Schoenecker, G. A. Belancik, B. E. Grabicka and K. S. Walton, *AIChE J.*, 2013, **59**, 1255-1262.
7. S. J. Garibay and S. M. Cohen, *Chem. Commun.*, 2010, **46**, 7700-7702.
8. G. E. Cmarik, M. Kim, S. M. Cohen and K. S. Walton, *Langmuir*, 2012, **28**, 15606-15613.
9. C. Wang, Z. Xie, K. E. deKrafft and W. Lin, *J. Am. Chem. Soc.*, 2011, **133**, 13445-13454.
10. K. Manna, T. Zhang and W. Lin, *J. Am. Chem. Soc.*, 2014, **136**, 6566-6569.
11. C. Wang, K. E. deKrafft and W. Lin, *J. Am. Chem. Soc.*, 2012, **134**, 7211-7214.
12. S. M. Cohen, *Chem. Rev.*, 2012, **112**, 970-1000.
13. M. Kim, J. A. Boissonnault, P. V. Dau and S. M. Cohen, *Angew. Chem. Int. Ed.*, 2011, **50**, 12193-12196.
14. P. V. Dau, M. Kim and S. M. Cohen, *Chem. Sci.*, 2013, **4**, 601-605.
15. A. Spek, *J. Appl. Crystallogr.*, 2003, **36**, 7-13.
16. H. Wu, T. Yildirim and W. Zhou, *J. Phys. Chem. Lett.*, 2013, **4**, 925-930.
17. S. Chavan, J. G. Vitillo, D. Gianolio, O. Zavorotynska, B. Civalleri, S. Jakobsen, M. H. Nilsen, L. Valenzano, C. Lamberti, K. P. Lillerud and S. Bordiga, *Phys. Chem. Chem. Phys.*, 2012, **14**, 1614-1626.
18. Q. Yang, V. Guillerm, F. Ragon, A. D. Wiersum, P. L. Llewellyn, C. Zhong, T. Devic, C. Serre and G. Maurin, *Chem. Commun.*, 2012, **48**, 9831-9833.
19. G. W. T. M. J. Frisch, H. B. Schlegel, G. E. Scuseria, M. A. Robb, J. R. Cheeseman, G. Scalmani, V. Barone, B. Mennucci, G. A. Petersson, H. Nakatsuji, M. Caricato, X. Li, H. P. Hratchian, A. F. Izmaylov, J. Bloino, G. Zheng, J. L. Sonnenberg, M. Hada, M. Ehara, K. Toyota, R. Fukuda, J. Hasegawa, M. Ishida, T. Nakajima, Y. Honda, O. Kitao, H. Nakai, T. Vreven, J. A. Montgomery, Jr., J. E. Peralta, F. Ogliaro, M. Bearpark, J. J. Heyd, E. Brothers, K. N. Kudin, V. N. Staroverov, R. Kobayashi, J. Normand, K. Raghavachari, A. Rendell, J. C. Burant, S. S. Iyengar, J. Tomasi, M. Cossi, N. Rega, J. M. Millam, M. Klene, J. E. Knox, J. B. Cross, V. Bakken, C. Adamo, J. Jaramillo, R. Gomperts, R. E. Stratmann, O. Yazyev, A. J. Austin, R. Cammi, C. Pomelli, J. W. Ochterski, R. L. Martin, K. Morokuma, V. G. Zakrzewski, G. A. Voth, P. Salvador, J. J. Dannenberg, S. Dapprich, A. D. Daniels, Ö. Farkas, J. B. Foresman, J. V. Ortiz, J. Cioslowski, and D. J. Fox, 2009.
20. http://wiki.wpi.edu/deskinsgroup/Density_of_States_-_CP2K.
21. M. K. Hazra, J. S. Francisco and A. Sinha, *J. Phys. Chem. A*, 2013, **117**, 11704-11710.
22. B. Wang, H. Huang, X.-L. Lv, Y. Xie, M. Li and J.-R. Li, *Inorg. Chem.*, 2014, **53**, 9254-9259.